

Ruano, M., Bedford, M., Kelemen, D., & Ferro, V. A. (2026). Establishing a chicken embryo model for studying infection control of a novel lipid nanoparticle. *International Journal of Pharmaceutics*, 690, Article 126569. <https://doi.org/10.1016/j.ijpharm.2026.126569>. For the purpose of open access, a CC BY 4.0 licence has been applied.

Establishing a chicken embryo model for studying infection control of a novel lipid nanoparticle

Marta Ruano^{1*}, Mike Bedford², Donald Kelemen³, Valerie A. Ferro¹

¹Strathclyde Institute of Pharmacy & Biomedical Sciences, University of Strathclyde, 161

Cathedral Street, Glasgow, G4 0RE, United Kingdom

²AB Vista, Woodstock Court, Marlborough, Wiltshire SN8 4AN, UK

³ABITEC Corporation, 501 W 1st Ave, Columbus, OH 43215, United States

*Address correspondence to:

E-mail: marta.ruano-aldea@strath.ac.uk (M.R.)

Keywords

CAM – Chorioallantoic Membrane, CEM – Chicken Embryo Model, Lipid Nanoparticles, Infection model, Antibiotic resistance

Highlights

- Monoglyceride-based LNPs show potent antibacterial activity *in vitro*.
- Complete growth inhibition achieved for *S. aureus* and *S. enteritidis*.
- CAM model optimized for infection and antimicrobial testing.
- LNP treatment improved embryo survival in bacterial infections.
- Fluorescent imaging enabled real-time infection and treatment tracking.

Ruano, M., Bedford, M., Kelemen, D., & Ferro, V. A. (2026). Establishing a chicken embryo model for studying infection control of a novel lipid nanoparticle. *International Journal of Pharmaceutics*, 690, Article 126569. <https://doi.org/10.1016/j.ijpharm.2026.126569>. For the purpose of open access, a CC BY 4.0 licence has been applied.

Abstract

The rise of antibiotic-resistant infections highlights the urgent need for alternative therapeutic strategies. Monoglyceride-based lipid nanoparticles (LNPs) offer both antimicrobial activity and the potential for controlled drug delivery. In this study, LNPs with diameters of 230–350 nm and ζ -potential of approximately -35 mV demonstrated high colloidal stability and strong antibacterial efficacy *in vitro*, achieving complete growth inhibition of *Staphylococcus aureus* (*S. aureus*) at 0.04 mg/mL and *Salmonella enterica* subsp. *enterica* serovar Enteritidis (*S. Enteritidis*) at 0.9 mg/mL. To bridge the gap between *in vitro* and *in vivo* evaluation, the chicken chorioallantoic membrane (CAM) model was optimized as a physiologically relevant platform to study infection progression and treatment response. Incubation temperature and humidity, inoculum concentration, infection site, and imaging conditions were refined to ensure reproducibility and minimize embryo variability. LNP administration improved embryo survival: *S. aureus* from 35% to 65%, and *S. Enteritidis* from 40% to 65% at 48 h post-inoculation.

Fluorescently labeled *Escherichia coli* JM105-GFP and Nile Red-tagged LNPs enabled real-time monitoring of infection and nanoparticle biodistribution using the IVIS Spectrum imaging system, with GFP intensity strongly correlating with bacterial density ($R^2 = 0.985$). At concentrations above 10^9 CFU/mL, *Escherichia coli* JM105-GFP was readily visualized despite the eggshell's autofluorescence.

This study establishes a reproducible CAM infection model for Gram-positive and Gram-negative bacteria and demonstrates the therapeutic potential of monoglyceride-based LNPs as localized antimicrobial agents.

Ruano, M., Bedford, M., Kelemen, D., & Ferro, V. A. (2026). Establishing a chicken embryo model for studying infection control of a novel lipid nanoparticle. *International Journal of Pharmaceutics*, 690, Article 126569. <https://doi.org/10.1016/j.ijpharm.2026.126569>. For the purpose of open access, a CC BY 4.0 licence has been applied.

1. Introduction

The increasing prevalence of antibiotic-resistant bacterial infections and associated poor treatment outcomes underscores the urgent need for alternative therapeutic strategies in both animals, such as in feed additives or veterinary applications, and humans. Conventional antibiotics, such as erythromycin, have been widely used to combat bacterial infections due to their well-established efficacy (Platon et al., 2022). Erythromycin, a macrolide antibiotic, inhibits bacterial protein synthesis by binding to the 50S ribosomal subunit, thereby preventing peptide chain elongation (Krawczyk et al., 2024). This mechanism selectively targets bacterial protein production without affecting mammalian protein synthesis (Vázquez-Laslop and Mankin, 2018), making erythromycin a valuable treatment option. At lower doses, erythromycin functions as a bacteriostatic agent, halting bacterial growth and reproduction, whereas at higher concentrations, it exhibits a bactericidal effect, directly killing bacteria (Byrne et al., 2020). However, prolonged or high-dose administration of erythromycin can lead to systemic toxicity and contribute to the development of bacterial resistance, limiting its long-term clinical utility (Zaidi, 2016). Therefore, novel approaches are essential to enhance efficacy while minimizing adverse effects (Cyphert et al., 2017). In both animal and human applications, such strategies may include smart drug delivery systems (e.g., encapsulation, nanoparticles), dose optimization based on pharmacodynamics/pharmacokinetics, and adjunctive therapies to mitigate toxicity (Platon et al., 2022; Zou et al., 2023).

Lipid nanoparticles (LNPs) have emerged as a promising drug delivery platform capable of improving the therapeutic profile of antibiotics. These nanoscale carriers offer several advantages, including controlled drug release, enhanced bioavailability, improved cellular uptake, and potential for targeted delivery. In addition, LNPs can protect encapsulated drugs from premature degradation, reduce off-target effects, and potentially enhance antimicrobial activity by facilitating interaction with bacterial membrane (Nath et al., 2024). Despite these advantages, optimizing the *in vivo* application of LNPs requires a physiologically relevant and reproducible infection model to evaluate their antimicrobial efficacy, biodistribution, and potential toxicity under biologically relevant conditions (Motsoene et al., 2023).

Ruano, M., Bedford, M., Kelemen, D., & Ferro, V. A. (2026). Establishing a chicken embryo model for studying infection control of a novel lipid nanoparticle. *International Journal of Pharmaceutics*, 690, Article 126569. <https://doi.org/10.1016/j.ijpharm.2026.126569>. For the purpose of open access, a CC BY 4.0 licence has been applied.

The chicken chorioallantoic membrane (CAM) model is a well-established *ex ovo* platform that offers a versatile and cost-effective alternative to traditional mammalian *in vivo* studies. Characterized by its extensive vascular network and ease of manipulation, the CAM model has been widely employed to study host-pathogen interactions in real time (Kalmar et al., 2015). It also serves as an effective system for assessing drug delivery mechanisms enabling the evaluation of biodistribution, penetration, and therapeutic efficacy of various formulations (Victorelli et al., 2020)). Furthermore, the CAM model provides critical insights into nanoparticle behavior in a living system, facilitating the study of biocompatibility, cellular uptake, and targeted delivery (“Nanoparticles characterization using the CAM assay,” 2019). Its accessibility, ethical advantages, and physiological relevance make it an indispensable tool for preclinical research.

In this study, we optimized the chicken embryo model to assess key parameters influencing infection establishment, aiming to develop a standardised protocol for future studies. Temperature, humidity, and egg fertility rates were monitored to ensure consistent embryo viability. The site of formulation application was carefully selected to maximize nanoparticle interaction with the CAM, while bacterial inoculation doses were optimized to determine the LD50 for both Gram-positive (*S. aureus*) and Gram-negative (*S. Enteritidis*), ensuring a reproducible infection model.

To systematically evaluate these factors, we employed a fluorescently labeled *Escherichia coli* JM105–GFP strain alongside a Nile Red-labeled LNP formulation, enabling simultaneous monitoring of bacterial proliferation, nanoparticle distribution, uptake, and potential antimicrobial effects. This approach allowed real-time tracking of infection dynamics and assessment of LNP therapeutic potential in a physiologically relevant setting.

Ruano, M., Bedford, M., Kelemen, D., & Ferro, V. A. (2026). Establishing a chicken embryo model for studying infection control of a novel lipid nanoparticle. *International Journal of Pharmaceutics*, 690, Article 126569. <https://doi.org/10.1016/j.ijpharm.2026.126569>. For the purpose of open access, a CC BY 4.0 licence has been applied.

2. Materials and methods

2.1. Materials

All lipids used for nanoparticle preparation were obtained from ABITEC Corporation (Columbus, OH, USA) and included glyceryl monooleate (GMO), glyceryl monolaurate (GML), glycerol glyceryl dibehenate (GDB), Capmul MCM (MCM), Capmul PG-8 (PG8), and Capmul PG-12 (PG12). Nile Red and Dextran–FITC were purchased from Sigma-Aldrich (St. Louis, MO, USA). Luria–Bertani (LB) broth and Mueller-Hinton broth (MHB) were purchased in Invitrogen (Carlsbad, CA, USA). The bacterial strains used were *Staphylococcus aureus* (*S. aureus*) ATCC 25923 (American Type Culture Collection, Manassas, VA, USA), and *Salmonella enterica* subsp. *enterica* serovar Enteritidis (*S. Enteritidis*) P125109 were kindly provided to Mike Bedford by the University of Nottingham. *Escherichia coli* JM105 (GFP) ATCC® 47016 (biosafety category 1), was provided by Dr. Liam Rooney (Strathclyde Institute of Pharmacy and Biomedical Sciences, University of Strathclyde). All other reagents were of analytical grade. Deionised water was prepared using a Milli-Q purification system (Millipore Sigma, Burlington, MA, USA).

2.2. Lipid nanoparticle preparation

Nanoparticles were fabricated using microfluidic mixing (Neonano™ system, Nanofluidics, CA, USA) combining a lipid phase and aqueous phase containing 1 mM deoxycholic acid in PBS (pH 7.4) (Ruano *et al.*, 2025). ERY-loaded nanoparticles (GDB4–ERY) and dye-labeled nanoparticles (GDB4–NR, GDB4–FITC) were generated under controlled conditions. Unencapsulated ERY was removed by centrifugal filtration. Detailed procedures for dye labeling, and encapsulation are provided in the Support Information.

2.3. Characterization

LNP size, PDI, and ζ -potential were measured by Dynamic Light Scattering. ERY and FITC encapsulation efficiencies were determined by LC–MS and UV–vis

Ruano, M., Bedford, M., Kelemen, D., & Ferro, V. A. (2026). Establishing a chicken embryo model for studying infection control of a novel lipid nanoparticle. *International Journal of Pharmaceutics*, 690, Article 126569. <https://doi.org/10.1016/j.ijpharm.2026.126569>. For the purpose of open access, a CC BY 4.0 licence has been applied.

spectroscopy, respectively. Full characterization methods are reported in the Support Information.

2.4. *In vitro* antimicrobial assays

S. aureus and *S. Enteritidis* were cultured in Mueller–Hinton broth (MHB) to exponential phase (OD₆₀₀ ~0.3). Minimum inhibitory concentrations (MIC₅₀) of the LNP formulations were determined by broth microdilution according to NCCLS and BSAC guidelines. Full details of bacterial culture conditions, MIC determination, and data analysis are provided in the Support Information.

2.5. Chicken species and egg preparation

Fertilized White Leghorn (WLH) eggs were sourced from the Roslin Institute (Edinburgh, UK) (Chintoan-Uta et al., 2016, 2015). Egg collection was coordinated to ensure optimal quality and consistency: fresh eggs laid the previous night were collected the following morning and transported to the laboratory facility. Eggs were delivered within two hours of leaving the Roslin Institute, wrapped in polystyrene to maintain temperature stability, allowing experimental procedures to commence immediately upon arrival.

2.5.1. Optimization of incubation conditions

Fertilized WLH eggs were incubated at 37°C with 45% relative humidity (ED0) in a controlled incubator (Brinsea OvaEasy 380 Advance EX Series II Automatic Egg Incubator). Eggs were placed horizontally in incubation trays (Brinsea, Weston-super-Mare, UK), and the incubator shelves were programmed to tilt alternately by 45° every 45 min. Temperature and humidity ranges (37–38 °C; 45–65% RH) were initially evaluated to maximize embryo viability and reproducibility.

2.5.2. Standardization of experiment duration

Ruano, M., Bedford, M., Kelemen, D., & Ferro, V. A. (2026). Establishing a chicken embryo model for studying infection control of a novel lipid nanoparticle. *International Journal of Pharmaceutics*, 690, Article 126569. <https://doi.org/10.1016/j.ijpharm.2026.126569>. For the purpose of open access, a CC BY 4.0 licence has been applied.

The experimental timeframe was aligned with CAM development and infection kinetics. Although embryos remain viable until embryonic day 14 (ED14), the CAM is fully developed by ED5–7, and infected embryos typically progress within 24–48 h. Accordingly, antimicrobial and LNP formulations were evaluated during embryonic days 7–9 (ED7–ED9). Extended monitoring to ED10–ED11 was performed exclusively during preliminary optimization experiments and was not used for efficacy or biocompatibility assessments.

2.5.3. Correlation between egg weight and fertility

Egg weight was recorded on day 0 (ED0) and day 3 (ED3) of incubation. Eggs were categorized into weight groups to assess potential effects on fertility, as egg size can influence embryonic viability and developmental consistency (Patra et al., 2016). Fertility was determined during the windowing procedure by visualising embryonic development and CAM vascularisation. The relationship between egg weight and fertility was evaluated by plotting the weight categories against the percentage of fertile eggs and analyzed using linear regression.

2.5.4. Application site of compounds

To evaluate whether embryo survival was influenced by the site of compound administration, three delivery locations were examined using the same concentration of kanamycin. The concentration (3 mg/mL) was selected based on its established bioactivity and confirmed non-toxicity under stereoscopic examination (Voicu et al., 2013).

2.5.4.1. Air sac application

The wide base of the egg (location of the air sac) was punctured using a commercial egg piercer (WMF 16.2 × 6.5 × 3 cm). The compound (10 µL) was introduced into the air sac with a sterile 23 G needle, allowing diffusion through the embryonic membranes.

2.5.4.2. Direct CAM application

Ruano, M., Bedford, M., Kelemen, D., & Ferro, V. A. (2026). Establishing a chicken embryo model for studying infection control of a novel lipid nanoparticle. *International Journal of Pharmaceutics*, 690, Article 126569. <https://doi.org/10.1016/j.ijpharm.2026.126569>. For the purpose of open access, a CC BY 4.0 licence has been applied.

The wide end of the egg was punctured to remove ~5 mL of albumen with a sterile 23 G needle, and the opening was sealed with 3M Scotch electrical tape. A window (2 cm × 1 cm × 2 cm) was then cut on the top of the egg beneath a strip of 25 mm 3M Scotch Magic tape. A 10 µL volume of the formulation was applied directly onto the vascularised CAM using a pipette.

2.5.4.3. O-ring-assisted CAM application

O-rings (Totally Seals® 5 mm × 2 mm (9 mm OD) green FKM (Viton™), 75A Shore hardness) were placed on the CAM to confine the exposure area. A 10 µL aliquot of formulation was dispensed within each O-ring to ensure localised and controlled deposition.

Embryo survival was assessed at 24 and 96 h post-application, and the influence of application site on viability was analysed.

2.5.5. Windowing and set-up

All procedures were performed under a Class II safety cabinet (BioMAT-2, Medical Air Technology, UK) to maintain sterility. Prior to windowing (ED3), eggs were transferred to a portable incubator with controlled temperature and humidity (Brinsea Maxi 24 EX Incubator). The eggshell site opposite the air sac was disinfected with 70% ethanol. A 2 × 1 cm window was created following the CAM inoculation procedure (see Section 2.5.4. Application site of compounds), sealed with tape with approximately 4 cm of 3M Scotch magic tape, leaving a small tab for ease of re-opening the window. Each egg was placed in a Fisherbrand™ 85 mL polystyrene antistatic weighing boat (85 × 85 × 24 mm) positioned inside an open 150 cm² tissue culture flask with a re-closable lid, which contained 100 mL of sterilised water to maintain humidity. Eggs were then returned to the incubator and kept in a horizontal position until day 7 (ED7).

2.5.6. Bacteria concentration

Two bacterial strains were used: Gram-negative *S. Enteritidis* and Gram-positive *S. aureus* (category 2). LD50 values, defined as the bacterial dose causing 50% embryo mortality, were calculated using the Reed and Muench method (Ramakrishnan, 2016;

Ruano, M., Bedford, M., Kelemen, D., & Ferro, V. A. (2026). Establishing a chicken embryo model for studying infection control of a novel lipid nanoparticle. *International Journal of Pharmaceutics*, 690, Article 126569. <https://doi.org/10.1016/j.ijpharm.2026.126569>. For the purpose of open access, a CC BY 4.0 licence has been applied.

Reed and Muench, 1938). Bacteria were cultured in MHB at 37°C to mid-to-late log phase (OD₆₀₀ 0.5–1.0), harvested by centrifugation, and resuspended to 1–3 × 10⁹ CFU/mL. Serial dilutions (10 µL) were applied to the CAM on ED7, with 6–8 embryos per dose; MHB-only controls were included. Windows were resealed, and embryos incubated horizontally at 37°C. Embryo viability was assessed at 24 and 48 h post-inoculation, with windows temporarily opened for evaluation. This control group established a benchmark for infection severity and evaluate treatment efficacy.

2.5.7. Treatments in the chicken embryo model

Experimental and control groups are summarized in Supporting Information (Tables S1–S2). Controls included non-treated embryos, buffer or bile salt controls, and formulations or antibiotics without infection. Treatment groups comprised free erythromycin (ERY), antibiotic-free formulations, and ERY-encapsulated formulations at defined concentrations. Treatments (10 µL) were applied directly to the CAM; windows were resealed, and embryos incubated at 37 °C. Viability was assessed at 24 and 48 h by monitoring vascular integrity, movement, and development to evaluate treatment efficacy and biocompatibility.

2.5.8. *E. coli* JM105 (GFP) preparation for IVIS imaging

E. coli JM105 (GFP) (~488 nm excitation, 509 nm emission) was used for real-time fluorescence monitoring of bacterial infection. Cultures were grown in LB broth at 37 °C with shaking (200 rpm) and verified for stable GFP expression on LB agar supplemented with 30% (w/w) fresh egg albumin. This albumin was collected from the eggs used to establish the infection model and was homogenously mixed into molten agar where the bacteria growth.

For CFU enumeration, cultures were serially diluted, plated on LB agar, and incubated at 37 °C for 24 h. Cells were harvested at OD₆₀₀ = 1.0 (~1 × 10¹⁰ CFU/mL), washed, and resuspended for serial dilutions. Fluorescence imaging (500/540 nm) was performed using an IVIS® Spectrum system (PerkinElmer Inc., Waltham, MA, USA),

Ruano, M., Bedford, M., Kelemen, D., & Ferro, V. A. (2026). Establishing a chicken embryo model for studying infection control of a novel lipid nanoparticle. *International Journal of Pharmaceutics*, 690, Article 126569. <https://doi.org/10.1016/j.ijpharm.2026.126569>. For the purpose of open access, a CC BY 4.0 licence has been applied.

with standardized exposure and binning parameters. samples were placed in a standardised imaging chamber, and images were acquired using the appropriate excitation/emission filter settings for GFP. Preset exposure times and binning parameters were applied to ensure consistency. Fluorescence intensity was quantified as radiance (photons/s/cm²/sr) using Living Image software, and a highly fluorescent colony was selected for subsequent infection studies.

Statistical analysis: Data were expressed as mean \pm standard deviation (SD). The effects of bacterial dose and strain group on embryo mortality were analysed by simple linear regression. Non-parametric comparisons between groups were assessed using the Kruskal–Wallis test.

3. Results

3.1. Lipid nanoparticle formulation and characterization

GDB4-based lipid nanoparticles (LNPs) were successfully prepared in blank (Ruano et al., 2025), drug-loaded, and fluorescently labelled forms. All formulations exhibited mean hydrodynamic diameters (D_h) in the range of approximately 230–260 nm and ζ -potential of approximately -35 mV, indicative of good colloidal stability (Lopes et al., 2019a, 2019b, 2016; Vandoolaeghe et al., 2009), in Support Information (Table S3). Incorporation of erythromycin (ERY) or fluorescent probes (FITC or Nile Red, NR) did not markedly affect particle size distribution or surface charge.

Long-term stability studies demonstrated that D_h remained stable over a storage period of up to 180 days, with no statistically significant differences observed among formulations ($H = 6.097$, $p = 0.107$; Fig. 1A). Only a marginal reduction in D_h was detected over time, suggesting limited molecular rearrangement within the lipid matrix rather than aggregation or phase separation. These findings are consistent with previous reports in which stable D_h and ζ -potential profiles were associated with the absence of nanoparticle fusion or instability (Jakubek et al., 2023; Markova et al., 2021). In contrast, statistically significant changes in ζ -potential were observed among formulations over time ($H = 17.47$, $p = 0.0006$; in Supporting Information, Fig. S1), with

Ruano, M., Bedford, M., Kelemen, D., & Ferro, V. A. (2026). Establishing a chicken embryo model for studying infection control of a novel lipid nanoparticle. *International Journal of Pharmaceutics*, 690, Article 126569. <https://doi.org/10.1016/j.ijpharm.2026.126569>. For the purpose of open access, a CC BY 4.0 licence has been applied.

all values remaining strongly negative, consistent with sustained electrostatic stabilization (Lopes et al., 2016; Mehnert, 2001).

Encapsulation efficiencies were high for both hydrophobic and hydrophilic cargos. ERY encapsulation efficiency reached approximately 95%, while FITC encapsulation was around 90%, indicating effective retention within the lipid matrix. These values are comparable to or exceed those reported for similar lipid-based nanocarriers and reflect strong compatibility between the lipid components and the encapsulated agents (Beloqui et al., 2016; Perrigue et al., 2021). Calibration curves and regression analyses confirming the robustness of the analytical methods are reported in Supporting Information (Fig. S2 and Fig. S3).

3.2. *In vitro* antibacterial activity

The antibacterial activity of the formulations was evaluated against representative Gram-positive (*S. aureus*) and Gram-negative (*S. Enteritidis*) bacteria is presented in detail in Supporting Information (Fig. S4). Blank GDB4 nanoparticles exhibited intrinsic antibacterial activity against *S. aureus*, achieving complete growth inhibition at 0.04 mg mL⁻¹, whereas *S. Enteritidis* displayed markedly lower sensitivity. Free ERY showed greater efficacy against *S. aureus* than *S. Enteritidis*, consistent with its known preference for Gram-positive organisms (Dinos, 2017). Notably, encapsulation of ERY within GDB4 nanoparticles significantly enhanced antibacterial performance against both strains, reducing MIC₅₀ values by more than 20-fold for *S. aureus* and five-fold for *S. Enteritidis* ($p < 0.05$).

Overall, these results confirm that the GDB4 lipid system provides a stable and versatile platform for drug encapsulation, offering both intrinsic antimicrobial properties and enhanced antibiotic efficacy. Detailed physicochemical data, calibration curves, and encapsulation analyses are provided in the Supporting Information (Table S3).

3.3. Optimization of the chicken embryo model

Ruano, M., Bedford, M., Kelemen, D., & Ferro, V. A. (2026). Establishing a chicken embryo model for studying infection control of a novel lipid nanoparticle. *International Journal of Pharmaceutics*, 690, Article 126569. <https://doi.org/10.1016/j.ijpharm.2026.126569>. For the purpose of open access, a CC BY 4.0 licence has been applied.

3.3.1. Effect of relative humidity (RH) on survival rate of untreated eggs

The effect of relative humidity (RH) on embryo viability was assessed at 37.5 °C, as no significant differences were detected between 37 °C and 38 °C ($p = 0.933$). Embryos were therefore incubated at the optimized temperature of 37.5 °C under three RH conditions (45%, 55%, and 65%), and survival was monitored up to embryonic day 10 (ED10). Data are summarized in **Fig.1**.

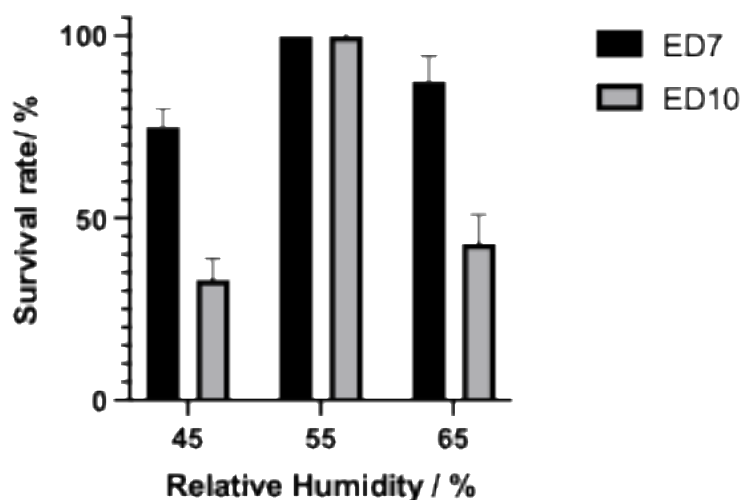


Fig.1. Effect of relative humidity on embryo viability. Survival rate (%) of chick embryos incubated at 37.5 °C under relative humidity conditions of 45%, 55%, and 65%. Data are presented as mean \pm SD ($n = 10$ embryos per group). Statistical differences among humidity conditions were assessed using the Kruskal–Wallis test.

Embryo survival at ED7 was 87.5%, compared with 58.7% at ED10 under 65% RH. Statistical analyses (unpaired t -test, Welch's correction, $p = 0.2999$; Kruskal–Wallis, $H = 0.286$, $p = 0.933$) showed no significant differences among humidity conditions, although descriptive data revealed reduced viability (<50%) at 45% and 65% RH. Embryos maintained at 55% RH showed 100% survival, confirming this as the optimal humidity for further experiments.

3.3.2. Correlation between egg weight and egg fertility

Ruano, M., Bedford, M., Kelemen, D., & Ferro, V. A. (2026). Establishing a chicken embryo model for studying infection control of a novel lipid nanoparticle. *International Journal of Pharmaceutics*, 690, Article 126569. <https://doi.org/10.1016/j.ijpharm.2026.126569>. For the purpose of open access, a CC BY 4.0 licence has been applied.

Egg weight has been proposed as a potential indicator of fertilisation success and early embryonic viability; however, this relationship remains inconsistently defined across experimental and production settings. To investigate whether egg weight influences fertility in our chicken embryo model, eggs were categorised into three weight groups—small (<50 g), medium (50–60 g), and large (>60 g)—and assessed for fertilisation success at day 0 and day 3 of incubation. **Fig.2** illustrates the correlation between egg weight categories and fertilisation outcomes obtained from multiple experimental batches.

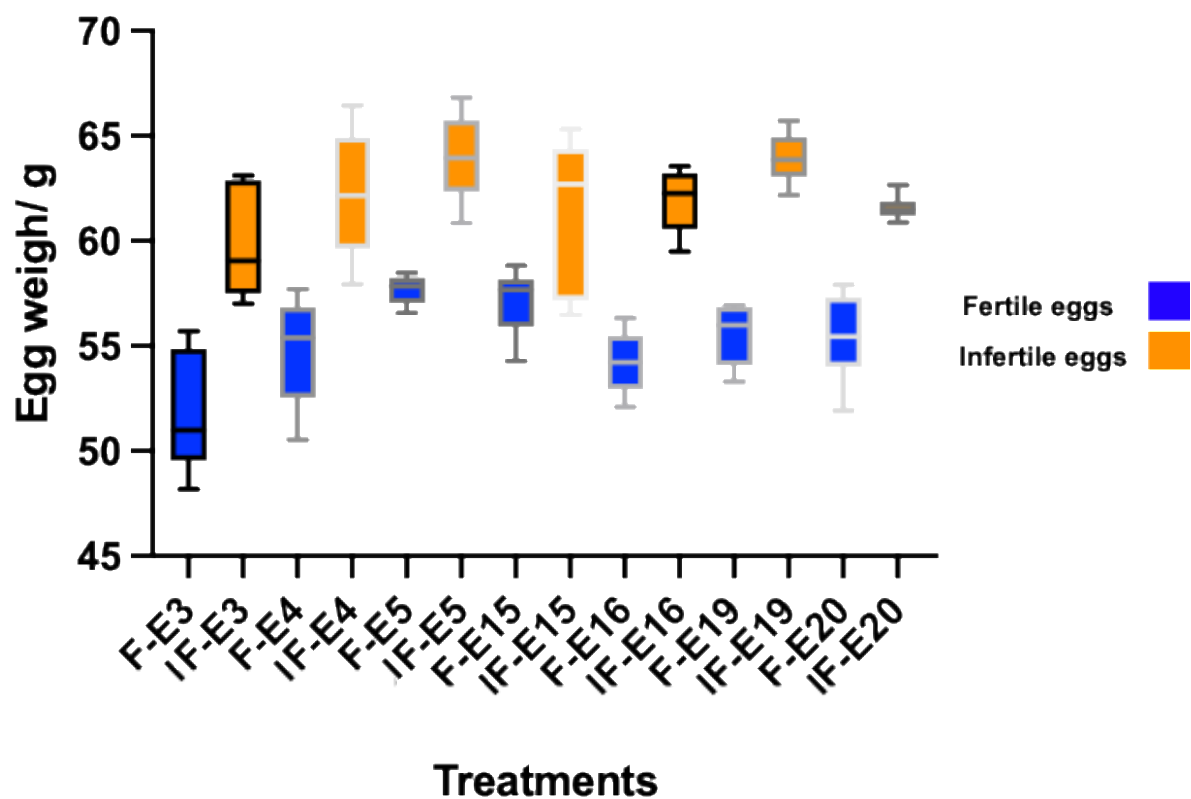


Fig.2. Fertility across standardised egg-weight groups. Fertility rates (%) are shown in blue and infertility rates (%) in orange for small (<50 g), medium (50–60 g), and large (>60 g) eggs. Statistical analysis was performed using the Kruskal–Wallis test ($H = 66.01$, $p < 0.0001$) followed by Dunn’s post hoc comparisons. Data represent mean \pm SD from 14 independent groups ($n = 84$).

Fertility differed significantly across the independent egg-weight groups ($H = 66.01$, $p < 0.0001$). Post-hoc comparisons showed that small eggs had significantly higher fertility than large eggs ($p < 0.0001$) and medium eggs also displayed higher fertility

Ruano, M., Bedford, M., Kelemen, D., & Ferro, V. A. (2026). Establishing a chicken embryo model for studying infection control of a novel lipid nanoparticle. *International Journal of Pharmaceutics*, 690, Article 126569. <https://doi.org/10.1016/j.ijpharm.2026.126569>. For the purpose of open access, a CC BY 4.0 licence has been applied.

than large eggs ($p < 0.0001$), while no significant difference was observed between small and medium eggs ($p > 0.05$). Although heavier eggs are often associated with more mature hens and larger yolk reserves, they also present a higher likelihood of structural shell irregularities and impaired gas exchange, which can compromise fertility and early embryonic development (Peebles and Brake, 1987).

3.3.3. Effect of treatment location on embryo survival

Fig.3. compares three administration routes evaluated at the primary assessment window (ED7) and during extended monitoring at ED11, which was performed only in preliminary optimization experiments and excluded from efficacy or biocompatibility analyses: (i) inoculation via the air sac using a 22-gauge needle, (ii) direct deposition on the CAM, and (iii) localized application within a Viton O-ring placed on the CAM. Each route was tested with 10 μ L of either bacterial inoculum or LNP formulation to assess survival outcomes and localization precision.

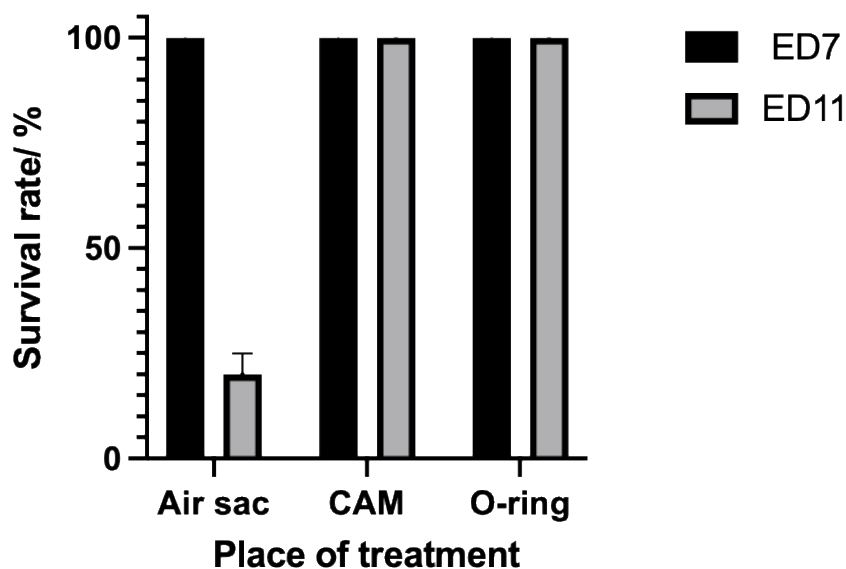


Fig.3. Influence of treatment location on chick embryo survival. Survival rate (%) of chick embryos at ED7 (primary evaluation window) and ED11 (extended monitoring performed only during preliminary optimization experiments; not included in efficacy or biocompatibility analyses) as a function of administration site. Data are presented as mean \pm SD ($n = 10$ per group). Statistical significance was assessed using the

Ruano, M., Bedford, M., Kelemen, D., & Ferro, V. A. (2026). Establishing a chicken embryo model for studying infection control of a novel lipid nanoparticle. *International Journal of Pharmaceutics*, 690, Article 126569. <https://doi.org/10.1016/j.ijpharm.2026.126569>. For the purpose of open access, a CC BY 4.0 licence has been applied.

Kruskal–Wallis test followed by pairwise Mann–Whitney U tests with Bonferroni correction.

Survival did not differ between treatment sites at ED7; however, by ED11, survival varied significantly across application routes (Kruskal–Wallis test, $H = 19.36$, $P < 0.001$). Pairwise Mann–Whitney U tests with Bonferroni correction confirmed significantly lower survival following air sac administration compared with both CAM and O-ring delivery ($P = 0.00055$ for both comparisons), while no difference was observed between CAM and O-ring groups ($P = 1.0$). Embryos treated via the air sac exhibited markedly reduced survival ($20\% \pm 5\%$), whereas CAM and O-ring application each achieved 100% survival (SD reflects replicate variability). The reduced viability associated with air sac administration likely reflects a combination of mechanical disruption and increased systemic exposure, which can lead to widespread distribution of the inoculum and heightened toxicity (Kue et al., 2015; Patiño-Morales et al., 2023). In contrast, CAM and O-ring delivery confine the formulation to a localized region, minimizing tissue damage and limiting systemic absorption, thereby improving embryo survival (Naik et al., 2018). Based on these observations, subsequent experiments employed O-ring–localized application to ensure controlled deposition and reproducible quantification of bacterial suspensions or formulations. Collectively, these findings highlight the critical influence of administration site on compound bioavailability and toxicity in the chick embryo model and reinforce the value of spatially controlled delivery strategies.

3.3.4. Influence of bacterial concentration and species

Serial bacterial dilutions ranging from 10^6 to 10^1 CFU per embryo were inoculated onto the CAM, and LD50s were calculated based on deaths that occurred through 24–48 h postinfection (**Fig.4**). All values represent the pooled results of independent experiments ($n = 8$), with eight embryos inoculated per bacterial dose.

Ruano, M., Bedford, M., Kelemen, D., & Ferro, V. A. (2026). Establishing a chicken embryo model for studying infection control of a novel lipid nanoparticle. *International Journal of Pharmaceutics*, 690, Article 126569. <https://doi.org/10.1016/j.ijpharm.2026.126569>. For the purpose of open access, a CC BY 4.0 licence has been applied.

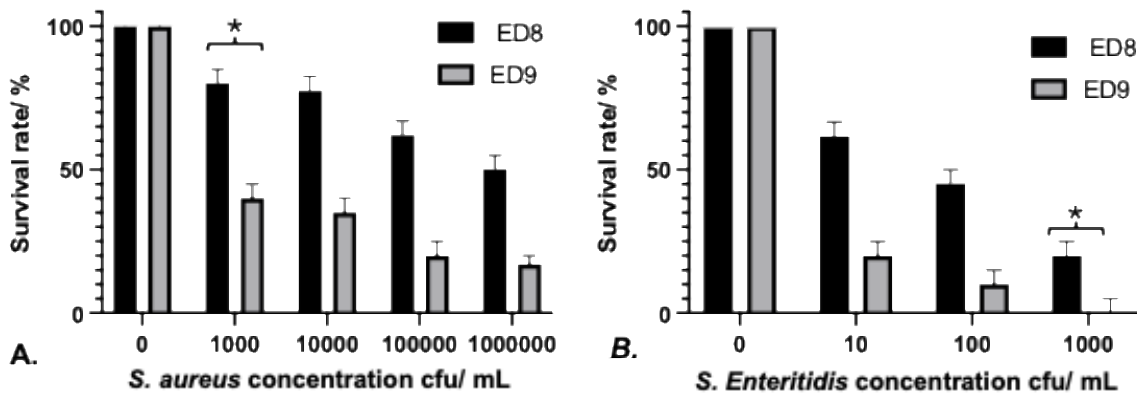


Fig.4. Dose-dependent effects of bacterial infection on chick embryo survival. Embryo survival (%) as a function of inoculated bacterial concentration at 24 and 48 h post-infection for (A) *S. Enteritidis* and (B) *S. aureus*. Data are presented as mean \pm SD from independent experiments ($n = 8$) with eight embryos per bacterial dose. Statistical analysis was performed using one-way ANOVA followed by Tukey's post-hoc test ($p < 0.05$). Asterisks indicate statistically significant differences between bacterial doses.

The LD₅₀ values differed between bacterial species, reflecting variations in virulence and host susceptibility in the chick embryo model (Dolka et al., 2022). For *S. Enteritidis*, a low inoculum of 1.5×10^1 CFU caused significant morbidity and mortality, indicating high pathogenicity consistent with previous reports (Dolka et al., 2022; Wang et al., 2025). In contrast, *S. aureus* required a higher dose of 1.5×10^3 CFU to achieve comparable effects, with 40% embryo survival at 48 h post-inoculation. One-way ANOVA followed by Tukey's post-hoc test ($p < 0.05$) revealed significant differences between bacterial doses for both species—for example, survival at 1.5×10^3 CFU differed significantly between *S. Enteritidis* and *S. aureus*—confirming that the dose-dependent trends were statistically meaningful. These findings highlight species-specific infection dynamics and underscore the importance of optimizing bacterial dosing in the CAM model to achieve reproducible and physiologically relevant outcomes for evaluating antimicrobial therapies.

3.3.5. Standard operating protocol

Ruano, M., Bedford, M., Kelemen, D., & Ferro, V. A. (2026). Establishing a chicken embryo model for studying infection control of a novel lipid nanoparticle. *International Journal of Pharmaceutics*, 690, Article 126569. <https://doi.org/10.1016/j.ijpharm.2026.126569>. For the purpose of open access, a CC BY 4.0 licence has been applied.

The optimized protocol involved incubating eggs at 37.5 °C and 55% relative humidity (RH), with experimental assessments conducted between embryonic days 7 and 9 (ED7–ED9). Final endpoints—including embryo survival, developmental progression, and antimicrobial efficacy—were recorded and compared with appropriate control groups, including untreated embryos and embryos treated with free antimicrobial agents. Treatment efficacy was primarily evaluated based on embryo mortality and visible signs of infection. **Table 1** summarizes the sequential steps used to establish the chick embryo infection model, including egg preparation, inoculation strategy, bacterial dose, incubation conditions, and embryo monitoring to ensure reproducibility.

Table 1. Stepwise procedure for establishing the final chick embryo infection model.

Day	Task	Description
0-3	Incubation and windowing	Eggs were incubated under controlled temperature and humidity. On ED3, ~5 mL of albumen was removed from the air sac to reduce internal pressure, and a sterile window was created on the eggshell for fertility assessment. After confirmation of fertility, the window was sealed with sterile tape to prevent contamination and evaporation. Eggs were placed in a weighing boat within a sealed flask containing 100 mL of sterile Milli-Q water to maintain high humidity. This hybrid <i>in ovo</i> – <i>ex ovo</i> setup involved a relatively large window (~one-third of the eggshell) to facilitate manipulation of O-rings and experimental procedures.
7	Inoculation and treatment	On ED7, two sterile O-rings were positioned on the CAM. A sublethal bacterial inoculum was applied within one O-ring, while LNP formulations or control solutions were applied to a separate O-ring to avoid direct interaction. Eggs were then returned to the incubator.
8-9	Primary evaluation window	During the 24–48 h post-inoculation period (ED8–ED9), embryos were monitored for mortality, developmental abnormalities, and treatment-related effects. Changes in growth or vascular architecture were documented using a stereomicroscope.

Ruano, M., Bedford, M., Kelemen, D., & Ferro, V. A. (2026). Establishing a chicken embryo model for studying infection control of a novel lipid nanoparticle. *International Journal of Pharmaceutics*, 690, Article 126569. <https://doi.org/10.1016/j.ijpharm.2026.126569>. For the purpose of open access, a CC BY 4.0 licence has been applied.

10-11*	Extended monitoring	*Performed only during preliminary optimization experiments; not included in efficacy or biocompatibility analyses.
--------	---------------------	---

In our optimized protocol, maintaining incubation at 37.5°C and 55% relative humidity provided stable embryonic development and minimized variability in infection outcome, consistent with previous studies (Dolka et al., 2022). The ED7–ED9 evaluation window was selected to balance CAM maturity, vascular accessibility, and embryo resilience (Dolka et al., 2022; Wang et al., 2025). Earlier inoculation (ED5–ED6) is associated with increased mortality (Wang et al., 2025), whereas later inoculation (ED10–ED12) can result in inconsistent infection establishment due to reduced CAM permeability (Castañeda et al., 2019).

The dual O-rings configuration, which spatially separates bacterial inoculation from treatment application, represents a refinement over conventional CAM infection models where both components are applied to the same site (Wang et al., 2025). This separation minimizes direct interference between inoculum and formulation, allowing more accurate assessment of therapeutic effects. In addition, the use of fluorescently labeled bacteria and nanoparticles enables non-invasive monitoring of infection progression and biodistribution, consistent with prior CAM-based imaging approaches (Castañeda et al., 2019).

Overall, this protocol provides a reproducible and ethically compliant *in vivo*-like platform for evaluating bacterial infections and antimicrobial therapies, while supporting the 3Rs principles (Replacement, Reduction, and Refinement) by reducing reliance on mammalian models.

3.4. Evaluation of LNP *irritation potential*

The Hen’s Egg Test–CAM (HET-CAM assay) is a well-established alternative to the Draize eye test for assessing irritation potential, mimicking the conjunctival tissue and enabling evaluation of vascular responses such as hyperemia, hemorrhage, and coagulation (Castañeda et al., 2019; De Araujo Lowndes Viera et al., 2022; Wang et

Ruano, M., Bedford, M., Kelemen, D., & Ferro, V. A. (2026). Establishing a chicken embryo model for studying infection control of a novel lipid nanoparticle. *International Journal of Pharmaceutics*, 690, Article 126569. <https://doi.org/10.1016/j.ijpharm.2026.126569>. For the purpose of open access, a CC BY 4.0 licence has been applied.

al., 2025). Although HET-CAM protocols recommend 300 μ L (National Institute of Environmental Health Sciences., 2006; Smail, 2024), validated protocol variants (Rivero et al., 2021) have used much smaller volumes (10 μ L) for assessing irritation in the CAM (Warncke et al., 2020), supporting the suitability of the 10 μ L dose employed in our study.

Fertilized chicken eggs at ED10 received 10 μ L of test substances applied to the CAM. Vascular responses were recorded over 5 min using a stereoscopic microscope (80 \times magnification), including hyperemia, hemorrhage, and coagulation (**Fig.5**).

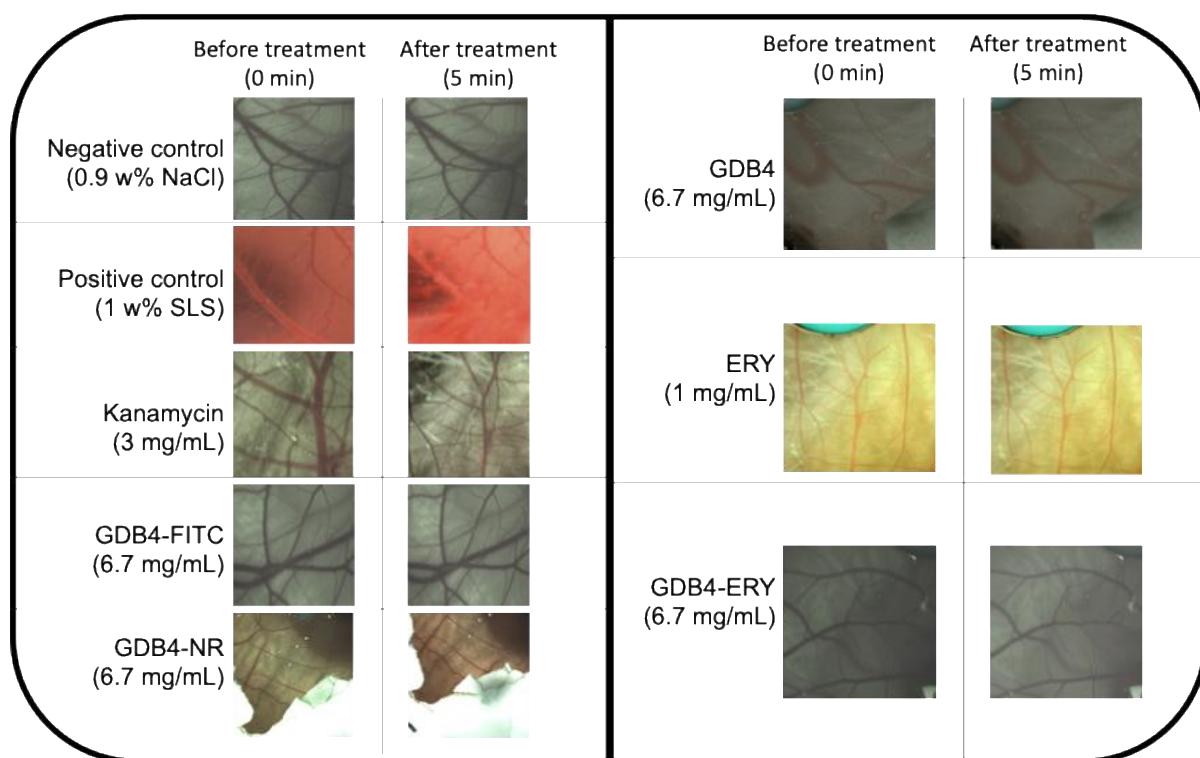


Fig.5. Stereomicroscopic images of the chick chorioallantoic membrane (CAM) before treatment and 5 min post-application. Vascular responses and membrane integrity are shown following exposure to controls (0.9% NaCl, 1% SLS), kanamycin, ERY, blank GDB4, and GDB4-based LNP formulations (GDB4-ERY, GDB4-FITC, GDB4-NR).

These images show preserved vascular integrity for all LNP formulations and antibiotics, indicating non-irritant behavior, while 1% SLS induced severe vascular

Ruano, M., Bedford, M., Kelemen, D., & Ferro, V. A. (2026). Establishing a chicken embryo model for studying infection control of a novel lipid nanoparticle. *International Journal of Pharmaceutics*, 690, Article 126569. <https://doi.org/10.1016/j.ijpharm.2026.126569>. For the purpose of open access, a CC BY 4.0 licence has been applied.

irritation. Each lesion was scored (Lotz, 2016; Luepke, 1985), with cumulative scores used in previous studies (Wang et al., 2025) to classify irritancy (0–0.9: non-irritant; 1–4.9: mild; 5–8.9: moderate; 9–21: severe). The mean score of four eggs was used for final classification. These responses, shown in **Table 2**, were graded based on predefined scoring criteria and are comparable to those observed in the conjunctiva of an albino rabbit’s eye (Chen et al., 2021).

Table 2. Representative images of the chick chorioallantoic membrane (CAM) before and 5 min after treatment with controls (0.9% NaCl, 1% SLS), antibiotics (kanamycin, ERY), and LNP formulations (blank GDB4, GDB4–FITC, GDB4–NR, GDB4–ERY).

Sample	CS	SD	Assessment
Negative control (0.9 w% NaCl)	0	0	Non-irritant
Positive control (1 w% SLS)	15	0.5	Severe irritant
Kanamycin (3 mg/mL)	0	0	Non-irritant
GDB4-FITC (6.7 mg/mL)	0	0	Non-irritant
GDB4-NR (6.7 mg/mL)	0	0	Non-irritant
GDB4 (6.7 mg/mL)	0	0	Non-irritant
ERY (1 mg/mL)	7	0.2	Moderate irritant
GDB4-ERY (6.7 mg/mL)	0	0	Non-irritant

Table 2 shows that controls behaved as expected: 0.9% NaCl was non-irritant (score 0), while 1% SLS induced severe irritation (score 15). Vascular responses were the earliest effects observed in the HET-CAM assay, appearing as transient vessel dilation and, in irritant controls, progressing to haemorrhage within ~20 s. ERY alone induced a moderate irritation response (score ≈ 7), while 1% SLS caused severe irritation (score ≈ 15). In contrast, Kanamycin (3 mg/mL), blank GDB4, GDB4-ERY, and GDB4 nanoparticles labelled with fluorescent dyes (FITC/NR) produced no vascular changes or hemorrhage (score 0), indicating good local tolerance at

Ruano, M., Bedford, M., Kelemen, D., & Ferro, V. A. (2026). Establishing a chicken embryo model for studying infection control of a novel lipid nanoparticle. *International Journal of Pharmaceutics*, 690, Article 126569. <https://doi.org/10.1016/j.ijpharm.2026.126569>. For the purpose of open access, a CC BY 4.0 licence has been applied.

therapeutic concentrations. These findings indicate that LNPs were well-tolerated at therapeutic concentrations, causing no vascular or membrane damage, in contrast to free ERY or SLS. The HET-CAM assay confirms the safety profile of these lipid nanoparticles, consistent with previous reports that phospholipid- and monoacylglyceride-based nanocarriers are generally non-irritant due to their biomimetic composition and low surfactant content (Schulze et al., 2023; Villani et al., 2025).

3.5. Treatment with bacteria and formulation

Fig.6 summarizes therapeutic efficacy in the chick CAM infection model, assessed using embryo survival as the primary endpoint. Embryos were infected with *S. aureus* or *S. Enteritidis* and treated with LNPs, kanamycin as a positive control, or left untreated as a negative control. Survival was monitored for 48 h post-infection and analyzed using log-rank and Gehan–Breslow–Wilcoxon tests, with eight embryos per group.

Ruano, M., Bedford, M., Kelemen, D., & Ferro, V. A. (2026). Establishing a chicken embryo model for studying infection control of a novel lipid nanoparticle. *International Journal of Pharmaceutics*, 690, Article 126569. <https://doi.org/10.1016/j.ijpharm.2026.126569>. For the purpose of open access, a CC BY 4.0 licence has been applied.

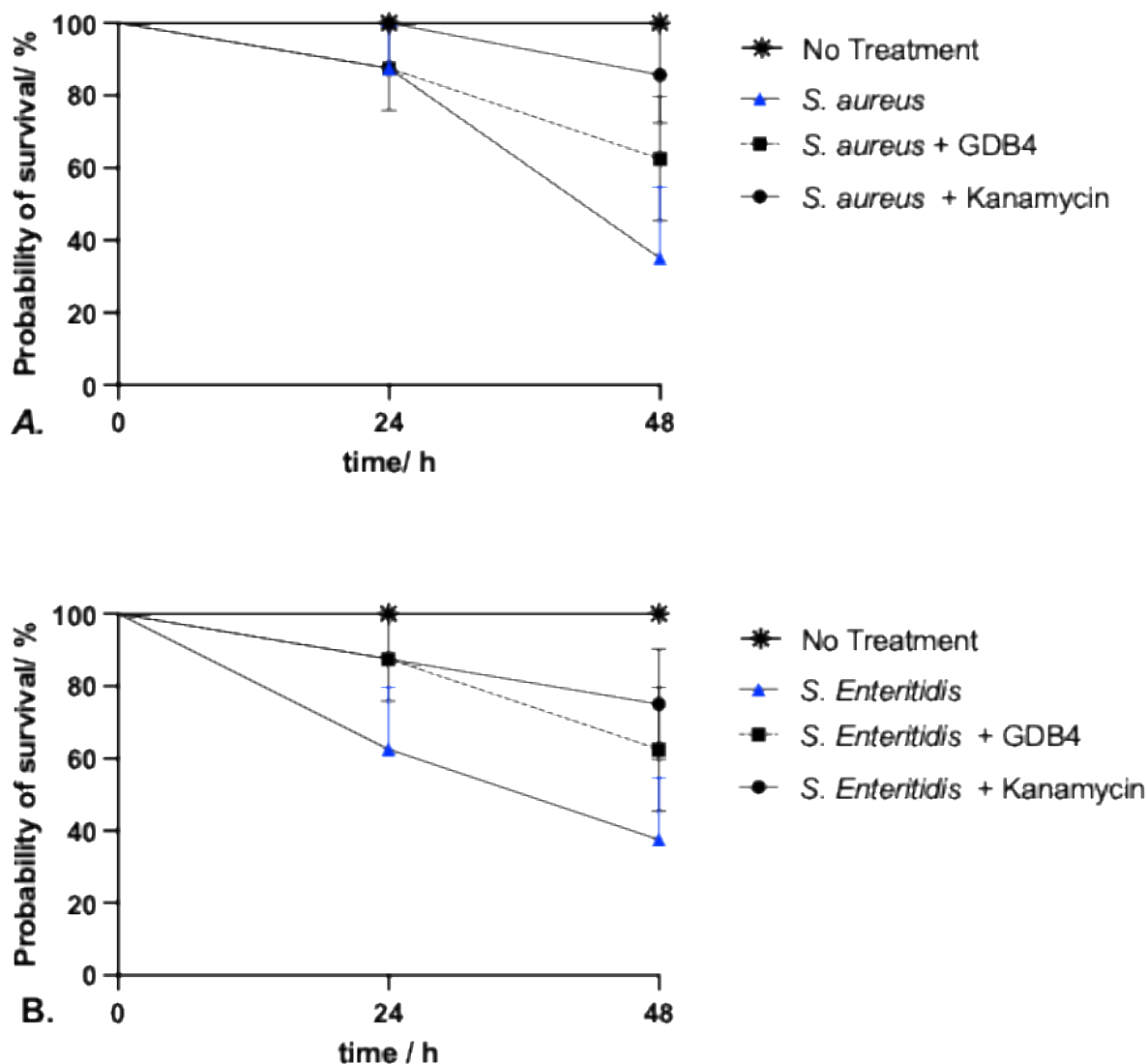


Fig.6. Survival of chick embryos following bacterial infection and treatment. Embryos infected with (A) *S. aureus* or (B) *S. Enteritidis* were treated with lipid nanoparticles (LNPs), kanamycin, or left untreated. Embryo survival (%) was monitored at 24 and 48 h post-treatment to evaluate therapeutic efficacy. Data are presented as mean \pm SD from independent experiments (n = 8).

LNP treatment improved embryo survival following infection with both bacterial species. In *S. aureus*-infected embryos, survival increased from 35% in untreated controls to 65% at 48 h post-inoculation (log-rank: $p = 0.0552$; Gehan–Breslow–Wilcoxon: $p = 0.0607$), positive trend in line with reports showing that lipid nanoparticles enhance antibiotic delivery and antimicrobial efficacy (Luepke, 1985). In

Ruano, M., Bedford, M., Kelemen, D., & Ferro, V. A. (2026). Establishing a chicken embryo model for studying infection control of a novel lipid nanoparticle. *International Journal of Pharmaceutics*, 690, Article 126569. <https://doi.org/10.1016/j.ijpharm.2026.126569>. For the purpose of open access, a CC BY 4.0 licence has been applied.

contrast, *S. Enteritidis*-infected embryos showed a statistically significant survival benefit, with survival increasing from 40% to 65% following LNP treatment (log-rank: $p = 0.0451$; Gehan–Breslow–Wilcoxon: $p = 0.0395$).

These data demonstrate that LNP administration enhances embryo survival after bacterial infection, with a more pronounced effect observed in *S. Enteritidis*, supporting the therapeutic potential of GDB4-based lipid nanocarriers in the CAM infection model.

3.6. IVIS imaging of bacteria

3.6.1. Measurement of *E. coli* JM105 (GFP) density and relative fluorescence intensity

The constitutive GFP expression in *E. coli* JM105 enabled fluorescence-based quantification of bacterial density. Bacterial concentrations were determined by CFU enumeration and correlated with IVIS fluorescence measurements. A strong linear relationship between fluorescence intensity and bacterial load was observed over the tested concentration range (data reported in the Supporting Information, Fig. S5), validating IVIS imaging as a reliable, non-invasive approach for quantifying bacterial load *in ovo*. This correlation was subsequently used to define the bacterial inoculum, after which *E. coli*–GFP was applied to the CAM using an O-ring to localise deposition and fluorescence was monitored longitudinally in **Fig.7**.

Ruano, M., Bedford, M., Kelemen, D., & Ferro, V. A. (2026). Establishing a chicken embryo model for studying infection control of a novel lipid nanoparticle. *International Journal of Pharmaceutics*, 690, Article 126569. <https://doi.org/10.1016/j.ijpharm.2026.126569>. For the purpose of open access, a CC BY 4.0 licence has been applied.

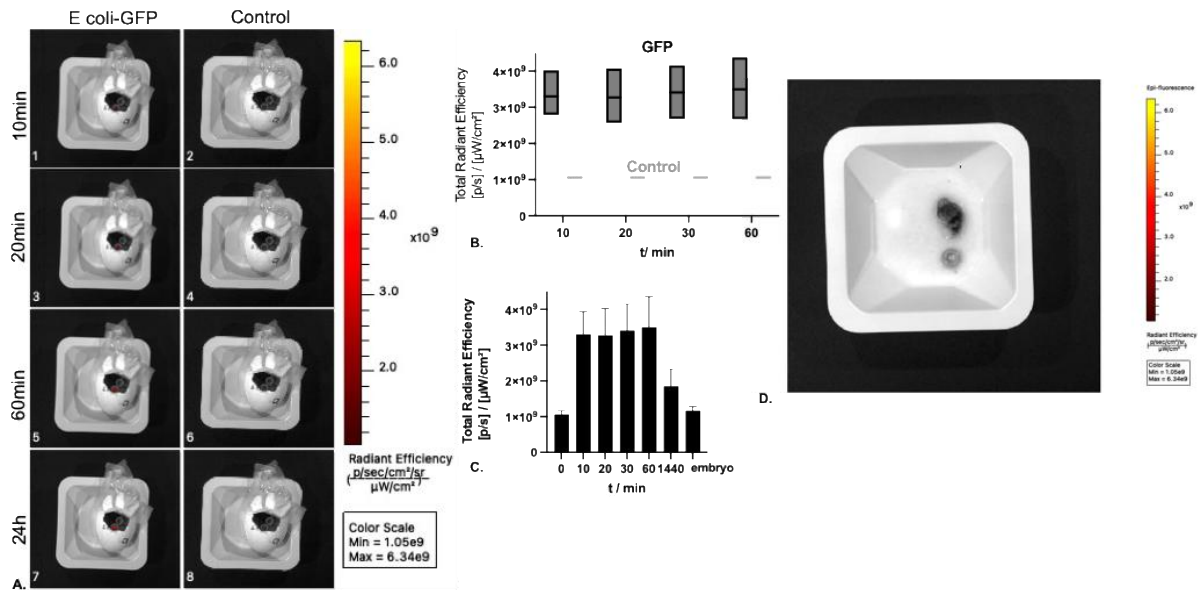


Fig.7. Temporal monitoring of GFP fluorescence on the CAM. (A) Representative IVIS images showing relative GFP signal intensity over time. A control empty O-ring was applied to the CAM for reference. (B) Quantitative correlation of fluorescence intensity with time post-application. (C) Fluorescence intensity (Radiant Efficiency [p/s] / [μW/cm²]) measured up to 24 h, including post-sacrifice readings. (D) Representative image of the embryo after sacrifice, confirming persistence of GFP signal.

Fig.7. A and D, were adjusted for brightness and contrast to highlight differences in fluorescence over time and versus control embryos. Color scaling indicates relative GFP intensity, enabling visual assessment of bacterial colonization. A control empty O-ring was imaged in parallel. Application of *E. coli* JM105 (GFP) resulted in a significant increase in fluorescence relative to baseline ($p < 0.0001$). For **Fig.7. B**, both one-sample t-test and Wilcoxon signed-rank test confirmed that mean radiance ($3.37 \times 10^9 \pm 1.02 \times 10^8$, $n = 4$) was significantly above zero ($t(3) = 65.86$, $p < 0.0001$; partial $\eta^2 = 0.9993$). At 24 h post-infection, **Fig.7. C**, mean radiance remained elevated ($2.51 \times 10^9 \pm 1.10 \times 10^9$, $n = 7$) and was again significantly greater than zero ($t(6) = 6.01$, $p = 0.0010$; partial $\eta^2 = 0.8574$), with Wilcoxon tests supporting these results ($p < 0.05$).

Ruano, M., Bedford, M., Kelemen, D., & Ferro, V. A. (2026). Establishing a chicken embryo model for studying infection control of a novel lipid nanoparticle. *International Journal of Pharmaceutics*, 690, Article 126569. <https://doi.org/10.1016/j.ijpharm.2026.126569>. For the purpose of open access, a CC BY 4.0 licence has been applied.

Time-course imaging demonstrated stable GFP signal up to 24 h, confirming bacterial viability and replication on the CAM. High reproducibility and large effect sizes (partial $\eta^2 > 0.85$) highlight the precision of IVIS fluorescence quantification, providing non-destructive, real-time monitoring of bacterial dynamics as an alternative to conventional CFU enumeration.

3.6.2. Fluorescent LNP distribution

3.6.2.1 Distribution assessment of GDB4-FITC on the CAM

The temporal distribution and retention of FITC-labeled GDB4 nanoparticles on the CAM were evaluated using longitudinal IVIS fluorescence imaging to assess surface association and persistence over time (**Fig.8**).

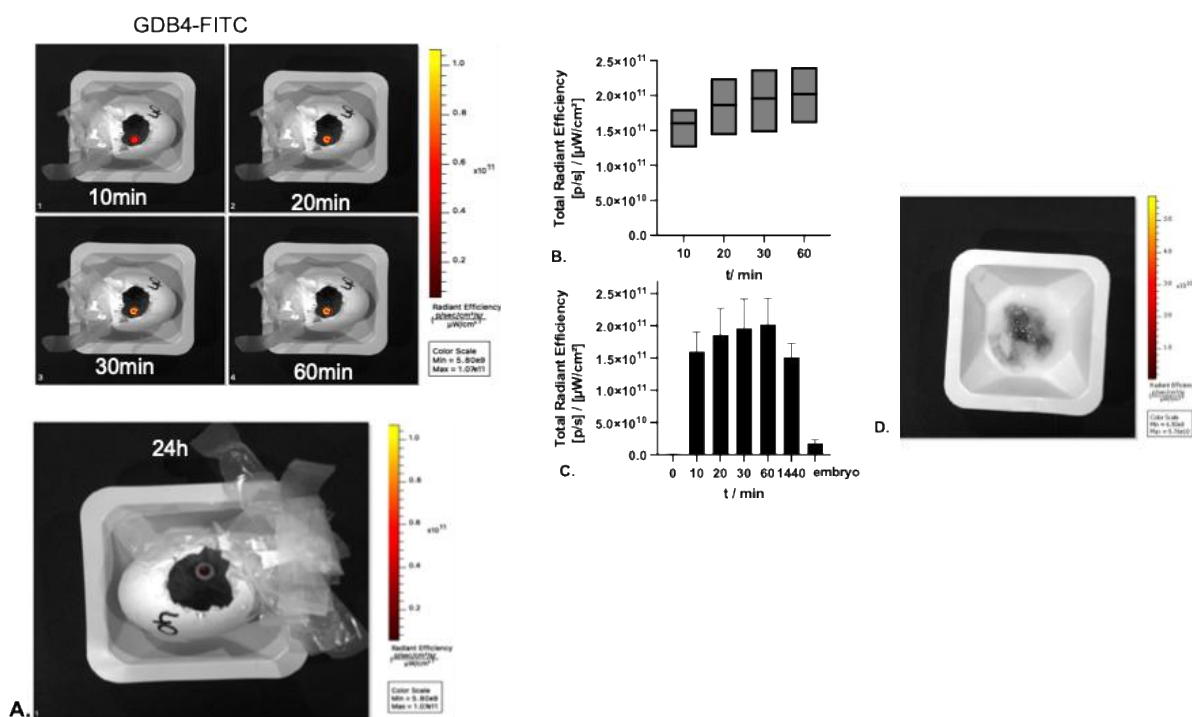


Fig.8. Temporal distribution of GDB4-FITC on the CAM. (A) Representative IVIS images showing progressive accumulation of GDB4-FITC over time. (B) Quantitative correlation between fluorescence signal and time, illustrating temporal dynamics of GDB4-FITC. (C) Fluorescence intensity (arbitrary units) measured up to 24 h, including post-sacrifice readings. Data represent mean \pm SD of ten independent

Ruano, M., Bedford, M., Kelemen, D., & Ferro, V. A. (2026). Establishing a chicken embryo model for studying infection control of a novel lipid nanoparticle. *International Journal of Pharmaceutics*, 690, Article 126569. <https://doi.org/10.1016/j.ijpharm.2026.126569>. For the purpose of open access, a CC BY 4.0 licence has been applied.

measurements (N = 3). (D) Embryo image after sacrifice confirming persistence of FITC signal.

Deposition of GDB4-FITC on the CAM generated a strong and persistent fluorescence signal over 24 h, with embryos remaining viable throughout the imaging period (**Fig.8. A**). Quantitative analysis revealed a mean radiance of $1.86 \times 10^{11} \pm 1.83 \times 10^{10}$ (n = 4), significantly above baseline (p = 0.0003), with a strong linear relationship between fluorescence intensity and time ($R^2 = 0.9928$).

Post-sacrifice measurements confirmed sustained fluorescence on the CAM surface ($1.31 \times 10^{11} \pm 8.49 \times 10^{10}$, n = 7; p = 0.0066), indicating prolonged association of FITC-labeled nanoparticles with the CAM and detectable signal retention following embryo dissection (**Fig.8. C, D**).

3.6.2.2 Distribution assessment of GDB4-NR on the CAM

The temporal distribution and retention of Nile Red-labeled GDB4 nanoparticles on the CAM were evaluated by IVIS fluorescence imaging to monitor both surface association and tissue penetration over 24 h (**Fig.9**).

Ruano, M., Bedford, M., Kelemen, D., & Ferro, V. A. (2026). Establishing a chicken embryo model for studying infection control of a novel lipid nanoparticle. *International Journal of Pharmaceutics*, 690, Article 126569. <https://doi.org/10.1016/j.ijpharm.2026.126569>. For the purpose of open access, a CC BY 4.0 licence has been applied.

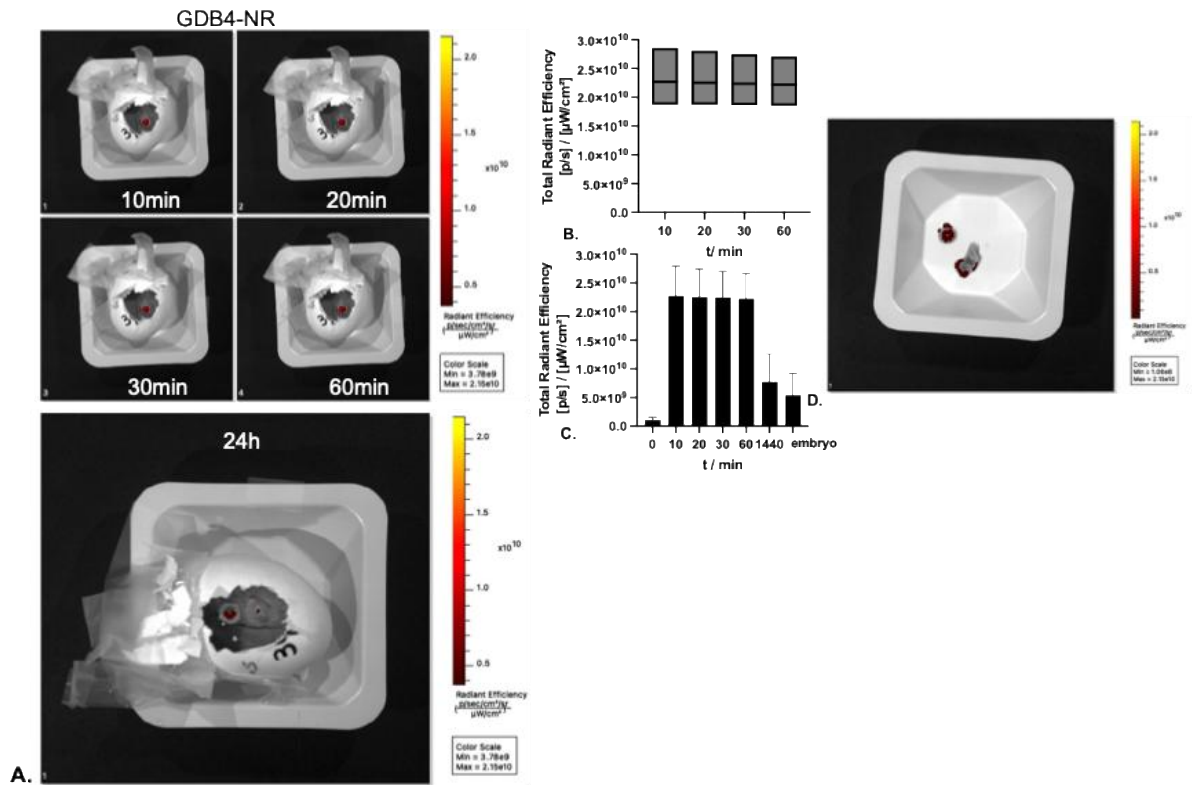


Fig.9. Temporal distribution of GDB4-NR on the CAM. (A) Representative IVIS images showing progressive increase in NR fluorescence over time. (B) Quantitative correlation between fluorescence signal and time, illustrating the dynamics of GDB4-NR. (C) Fluorescence intensity (Radiant Efficiency [p/s] / [μW/cm²]) measured up to 24 h, including post-sacrifice readings. Data represent mean ± SD of ten independent measurements (N = 3). (D) Embryo image after sacrifice confirming persistence of NR signal.

Fluorescence imaging of embryos treated with GDB4-NR revealed a strong, persistent signal throughout the 24 h period, with embryos remaining viable (**Fig.9. A**). Quantitative analysis indicated a mean radiance of $2.25 \times 10^{10} \pm 2.15 \times 10^8$ (n = 4), significantly above baseline (p < 0.0001), confirming robust nanoparticle retention (**Fig.9. B**).

Post-sacrifice imaging showed residual NR fluorescence within the embryo, suggesting partial tissue penetration (**Fig.9. C, D**). In comparison with GDB4-FITC,

Ruano, M., Bedford, M., Kelemen, D., & Ferro, V. A. (2026). Establishing a chicken embryo model for studying infection control of a novel lipid nanoparticle. *International Journal of Pharmaceutics*, 690, Article 126569. <https://doi.org/10.1016/j.ijpharm.2026.126569>. For the purpose of open access, a CC BY 4.0 licence has been applied.

which predominantly remained on the CAM surface, GDB4-NR exhibited stronger and more stable fluorescence within tissues, consistent with the lipophilic nature of Nile Red versus the hydrophilic properties of FITC (Buhr et al., 2020; Das et al., 2021).

3.6.2.3 Dual Bacteria-LNP tracking

Concurrent bacterial colonization and nanoparticle biodistribution were evaluated using time-resolved fluorescence imaging following localized application of *E. coli* JM105 (GFP) and GDB4-NR to separate O-rings (**Fig.10.**).

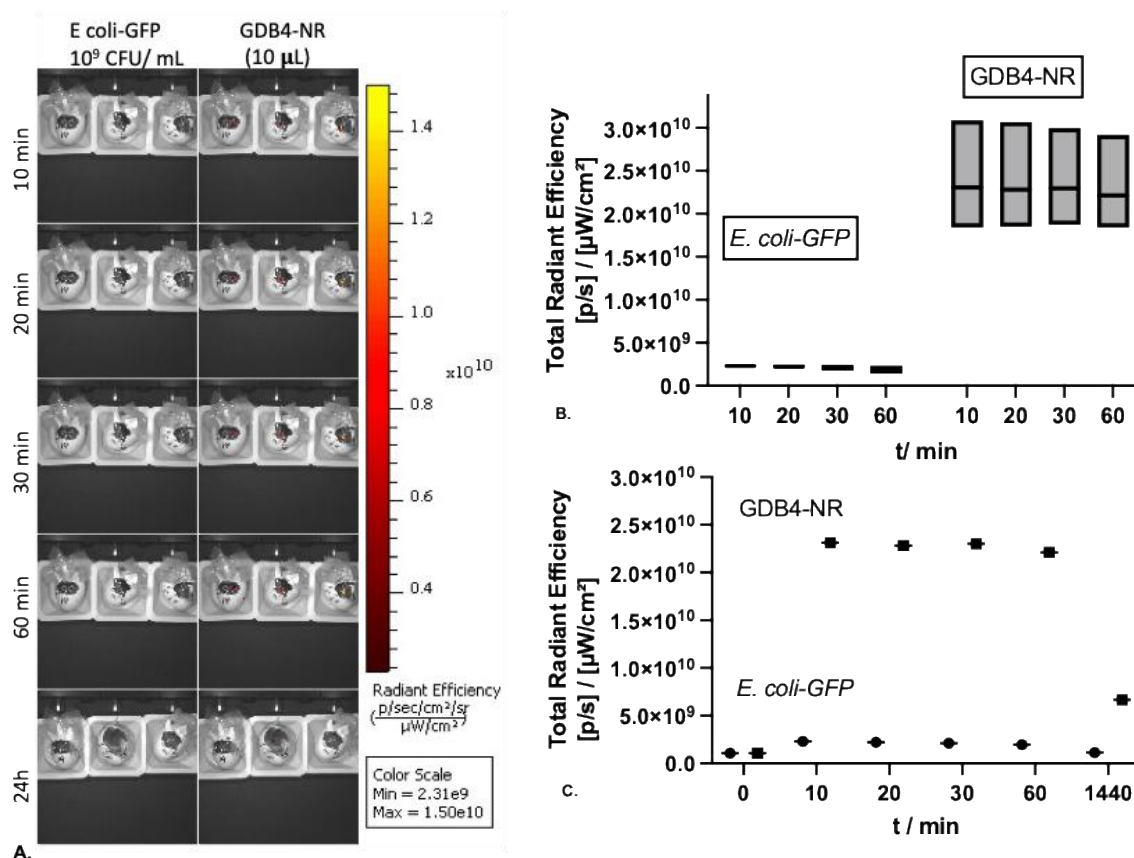


Fig.10. Dual tracking of bacterial infection and nanoparticle biodistribution. (A) Representative IVIS images of chick embryos infected with *E. coli* JM105 (GFP) and treated with GDB4-NR over time and at 24 h post-infection, confirming bacterial viability and colonization. (B) Fluorescence intensity of *E. coli* JM105 (GFP) and GDB4-NR recorded at 10-minute intervals for 30 min, with an additional measurement

Ruano, M., Bedford, M., Kelemen, D., & Ferro, V. A. (2026). Establishing a chicken embryo model for studying infection control of a novel lipid nanoparticle. *International Journal of Pharmaceutics*, 690, Article 126569. <https://doi.org/10.1016/j.ijpharm.2026.126569>. For the purpose of open access, a CC BY 4.0 licence has been applied.

at 60 min (N = 3). (C) Time-course monitoring of fluorescence signals from GFP bacteria and NR-labeled nanoparticles, including 24 h post-treatment measurements.

Mean total radiant efficiency ($[p/s]/[\mu W\text{ cm}^{-2}]$) was compared using an unpaired t-test with Welch's correction for unequal variances significantly showing higher for GFP-expressing bacteria (8.50×10^{10}) compared with NR-labeled nanoparticles (1.11×10^{10} ; $t(15.8) = 63.0$, $p < 0.0001$, $\eta^2 = 0.9960$), with unequal variance confirmed ($F(14,14) = 15.44$, $p < 0.0001$). Time-course imaging (**Fig.10. C**) showed that both bacteria and nanoparticles penetrated the embryo within 24 h, consistent with partial systemic distribution. This aligns with previous reports of enhanced retention of lipid nanoparticles in vascularized membranes due to nanoparticle–lipid affinity (Butler et al., 2022). These results highlight the potential of GDB4–NR as long-circulating carriers for sustained delivery and imaging. Future studies will require advanced imaging in more developed embryos to determine precise tissue localization during organogenesis.

4. Discussion

This study demonstrates the successful development and biological evaluation of GDB4 LNPs as a versatile platform for localized antibiotic delivery in a chick embryo infection model. The GDB4 LNPs exhibited high physicochemical stability, efficient drug loading, intrinsic antibacterial activity, biocompatibility, and in vivo efficacy, highlighting their potential as versatile antimicrobial carriers. Physicochemical characterization (Table S1; Fig. S1-S3) revealed uniformly dispersed nanoparticles with moderate polydispersity, and ζ -potential values indicative of good colloidal stability in monoglyceride-based nanosystems (Ruano et al., 2025). Incorporation of erythromycin (ERY) or fluorescent probes (FITC or NR) did not alter particle size or surface charge, and long-term storage studies indicated structural robustness and absence of aggregation or phase separation. These findings align with previous reports describing the stabilizing effects of long-chain saturated monoacylglycerides

Ruano, M., Bedford, M., Kelemen, D., & Ferro, V. A. (2026). Establishing a chicken embryo model for studying infection control of a novel lipid nanoparticle. *International Journal of Pharmaceutics*, 690, Article 126569. <https://doi.org/10.1016/j.ijpharm.2026.126569>. For the purpose of open access, a CC BY 4.0 licence has been applied.

in lipid nanoparticles (Markova et al., 2021; Mehnert, 2001; Perrigue et al., 2021; Vauthier and Bouchemal, 2009).

High encapsulation efficiencies for both ERY and FITC–dextran demonstrated the ability of the GDB4 matrix to incorporate hydrophobic and moderately hydrophilic compounds (Lakic et al., 2025; Singh and Nayak, 2023). Microfluidic production ensured uniform nanoparticle formation, narrow size distribution, and consistent drug loading, supporting compatibility with high-precision pharmaceutical manufacturing workflows (Jung et al., 2025).

Antibacterial evaluation indicated that blank GDB4 nanoparticles selectively inhibited Gram-positive bacteria, likely due to membrane-disrupting properties of medium- and long-chain monoglycerides (Meikle et al., 2021; Ruano et al., 2025), whereas Gram-negative bacteria were less affected. Encapsulation of ERY markedly enhanced antimicrobial efficacy against both Gram-positive and Gram-negative strains, consistent with improved drug penetration, sustained release, and enhanced local accumulation provided by lipid carriers (Aljihani et al., 2020; Lakic et al., 2025; Singh and Nayak, 2023). These findings agree with previous studies showing improved antibiotic activity and host survival using lipid nanocarriers in *Galleria mellonella* and zebrafish infection models (Gomes and Mostowy, 2020; Villani et al., 2025). Differential responses between Gram-positive (*S. aureus*) and Gram-negative (*S. Enteritidis*) bacteria likely reflect structural differences: nanoparticles can overcome the outer membrane of Gram-negative bacteria via membrane fusion (Modi et al., 2023), whereas *S. aureus* biofilms may hinder antibiotic diffusion (Das et al., 2021).

Optimization of the CAM model was critical for robust *in vivo* evaluation of antimicrobial GDB4 LNPs. While the CAM assay has been widely employed for angiogenesis, tumor growth, and toxicity testing (Kovacevic et al., 2011), standardized protocols for bacterial infection remain limited, leading to variability across studies (Jacobson et al., 2015). The optimized protocol described, maximised embryo survival (Dolka et al., 2022). The ED7–ED9 evaluation window was selected to balance full CAM vascular maturity with robust embryo viability, (De Souza et al., 2024; Dhayer et al., 2024), providing reproducible infection establishment while minimizing variability and non-

Ruano, M., Bedford, M., Kelemen, D., & Ferro, V. A. (2026). Establishing a chicken embryo model for studying infection control of a novel lipid nanoparticle. *International Journal of Pharmaceutics*, 690, Article 126569. <https://doi.org/10.1016/j.ijpharm.2026.126569>. For the purpose of open access, a CC BY 4.0 licence has been applied.

specific embryo mortality. Dual O-ring inoculation allowed spatial separation of bacterial inoculum and treatments, improving reproducibility (García-Gareta et al., 2020; Ranghar et al., 2013).

Infection outcomes were species-specific, with *S. Enteritidis* causing lethality at lower inocula than *S. aureus*, consistent with its known aggressive systemic infection profile (García-Gareta et al., 2020; Hemmati et al., 2023; Kundeková et al., 2021). Fluorescent labeling of both bacteria and nanoparticles enabled non-invasive, real-time monitoring of infection progression and biodistribution, supporting reproducibility while reducing the need for destructive sampling (Castañeda et al., 2019).

Biocompatibility assessment via HET-CAM confirmed that GDB4 LNPs were non-irritant, whereas free ERY induced mild vascular effects, highlighting the safety of the lipid matrix (Chen et al., 2021; Schulze et al., 2023; Wang et al., 2025; Warncke et al., 2020). *In vivo* efficacy was demonstrated by improved embryo survival following GDB4-ERY treatment, increasing from ~35–40% to 65% against both Gram-positive and Gram-negative infections (Abo-zeid et al., 2021; Hemmati et al., 2023; Lotz, 2016; Villani et al., 2025). This improvement indicates that encapsulation enhances drug bioavailability and therapeutic effect while avoiding toxicity.

Fluorescence imaging enabled non-destructive, real-time monitoring of both bacteria and nanoparticles. GFP fluorescence correlated with CFU counts, validating bacterial quantification (Gomes and Mostowy, 2020; Modi et al., 2023; Valdivia et al., 1996). GDB4-FITC primarily remained on the CAM surface, gradually accumulating over 24 h, whereas GDB4-NR produced a strong, relatively stable signal, indicating partial tissue penetration and systemic distribution (Buhr et al., 2020; Das et al., 2021; Klymchenko et al., 2021; Vairo et al., 2020). Fluorescence remained confined within O-ring boundaries, confirming spatially localized deposition and reproducible measurements (Warncke et al., 2020).

Dual imaging demonstrates the CAM's versatility for studying host–pathogen–nanocarrier interactions and supports future kinetic and pharmacological studies

Ruano, M., Bedford, M., Kelemen, D., & Ferro, V. A. (2026). Establishing a chicken embryo model for studying infection control of a novel lipid nanoparticle. *International Journal of Pharmaceutics*, 690, Article 126569. <https://doi.org/10.1016/j.ijpharm.2026.126569>. For the purpose of open access, a CC BY 4.0 licence has been applied.

(Barnoy et al., 2017; González-Fernández et al., 2021; Niamprem et al., 2019; Warncke et al., 2020).

Overall, these results establish GDB4 LNPs as a versatile, stable, and biocompatible nanocarrier system. The optimized CAM infection model combined with IVIS imaging provides a robust, reproducible platform for preclinical evaluation of antimicrobial nanotherapeutics.

5. Future directions

Building on these results, future studies should aim to further enhance the utility and translational relevance of the CEM platform. First, correlating fluorescence-based LNP and bacterial distribution with histological and molecular analyses will provide deeper insights into tissue-level localisation and mechanistic interactions. Extending the model to older embryos with more developed organs could enable organ-specific imaging, supporting studies on pharmacokinetics and targeted delivery.

Moreover, further work should explore co-encapsulation strategies, release kinetics under physiological conditions, and pharmacodynamic and toxicity profiles in higher animal models to improve preclinical relevance. Standardisation of infection doses, imaging parameters, and quantitative analysis pipelines will be critical to reduce inter-experimental variability and enhance reproducibility. Co-delivery of multiple therapeutics or imaging markers using functionalised LNPs could allow investigation of combinatorial and synergistic antimicrobial effects.

With these refinements, the CEM–IVIS platform has the potential to become a cornerstone model in nanotoxicology, antimicrobial drug discovery, and translational nanomedicine. It provides mechanistic insights into host–pathogen interactions, nanoparticle behavior, and therapeutic efficacy while adhering to the principles of the 3Rs (Replacement, Reduction, Refinement), supporting the development of next-generation nanotherapeutics.

Ruano, M., Bedford, M., Kelemen, D., & Ferro, V. A. (2026). Establishing a chicken embryo model for studying infection control of a novel lipid nanoparticle. *International Journal of Pharmaceutics*, 690, Article 126569. <https://doi.org/10.1016/j.ijpharm.2026.126569>. For the purpose of open access, a CC BY 4.0 licence has been applied.

6. Conclusion

This study demonstrates that the chick embryo model (CEM) is a robust, versatile, and ethical platform for evaluating antimicrobial efficacy, host–pathogen interactions, and nanocarrier biodistribution. Integration of the CAM assay with IVIS imaging enabled real-time, non-invasive monitoring of bacterial infection dynamics, LNP behaviour, and therapeutic performance in a living system.

The GDB4 LNPs displayed uniform particle sizes (230–350 nm), moderate polydispersity, and ζ -potential of approximately -35 mV, indicating high physicochemical stability. Both hydrophobic ERY and moderately hydrophilic FITC cargos were efficiently encapsulated and stably retained, demonstrating the suitability of the LNPs for diverse payloads. Antibacterial studies confirmed selective intrinsic activity against Gram-positive bacteria and enhanced efficacy of ERY-loaded LNPs against both Gram-positive and Gram-negative strains.

Optimization of the CEM, including dual O-ring inoculation and controlled environmental conditions, allowed reproducible spatial delivery of bacteria and nanoparticles while minimizing interference. Biocompatibility assessment via HET-CAM confirmed that GDB4 formulations were non-irritant, with no haemorrhage, hyperaemia, or coagulation observed, supporting their safety for localized delivery. Collectively, these findings validate the CEM–IVIS platform as a scalable and cost-effective alternative to traditional in vitro or mammalian infection models for early-stage evaluation of nanotherapeutics.

7. Acknowledgements

M.R. acknowledges support through the Knowledge Transfer Partnership (KTP) project that was developed between AB Vista, ABITEC Corporation, and the University of Strathclyde. M.R would like to thank Dr. Muattaz Hussain and Dr. Nikita Jain for providing training on IVIS imaging, and Dr. Liam Rooney for supplying the bacterial strains and offering valuable guidance and technical advice on their cultivation.

8. Glossary

Ruano, M., Bedford, M., Kelemen, D., & Ferro, V. A. (2026). Establishing a chicken embryo model for studying infection control of a novel lipid nanoparticle. *International Journal of Pharmaceutics*, 690, Article 126569. <https://doi.org/10.1016/j.ijpharm.2026.126569>. For the purpose of open access, a CC BY 4.0 licence has been applied.

AMP – Antimicrobial peptides

AR – Antibiotic resistance

BSA – Bovine Serum Albumin

CAM – Chorioallantoic membrane

C. albicans – *Candida albicans*

CFU – Colony Forming Units

CEM – Chick embryo model

DDS – Drug delivery systems

DNA – Deoxyribonucleic Acid

DLS – Dynamic Light Scattering

ED – Embryonic day

ELISA – Enzyme-Linked Immunosorbent Assays

E. coli JM105 (GFP) - *Escherichia coli* JM105 (GFP) ATCC® 47016

ERY – Erythromycin

FITC – Fluorescein Isothiocyanate

GFP – Green Fluorescent Protein

HET-CAM – Hen's Egg Test on the Chorioallantoic Membrane

HPLC – High-Performance Liquid Chromatography

IgM/IgY – Immunoglobulin M / Immunoglobulin Y

IS - Irritation score

IVIS – *In Vivo* Imaging System

LNP – Lipid nanoparticles

MDR – Multidrug resistance

MIC – Minimum Inhibitory Concentration

MTT – 3-(4,5-dimethylthiazol-2-yl)-2,5-diphenyltetrazolium bromide

NP – Nanoparticle

NR – Nile Red

P. aeruginosa – *Pseudomonas aeruginosa*

PBS – Phosphate-Buffered Saline

PEG – Polyethylene Glycol

PDI – Polydispersity Index

RH – Relative humidity

Ruano, M., Bedford, M., Kelemen, D., & Ferro, V. A. (2026). Establishing a chicken embryo model for studying infection control of a novel lipid nanoparticle. *International Journal of Pharmaceutics*, 690, Article 126569. <https://doi.org/10.1016/j.ijpharm.2026.126569>. For the purpose of open access, a CC BY 4.0 licence has been applied.

RNA – Ribonucleic acid

S. aureus – *Staphylococcus aureus*

S. Enteritidis - *Salmonella enterica* subsp. *enterica* serovar Enteritidis

SLN – Solid lipid nanoparticle

SDS-PAGE – Sodium Dodecyl Sulphate Polyacrylamide Gel Electrophoresis

TEM – Transmission Electron Microscopy

UV-Vis – Ultraviolet-Visible Spectroscopy

ZP – ζ -potential

Author contributions

MR: Conceptualization, Investigation, Writing-original draft, Writing-review & editing.

VF: Conceptualization, Investigation, Writing-original draft, Writing-review & editing.

MB: Validation, Supervision, DK: Validation, Supervision. All authors read and approved the submitted version.

Conflicts of interest

The authors declare that they have no conflicts of interest.

Ethical approval

Not applicable.

Consent to participate

Not applicable.

Consent to publication

Not applicable.

Availability of data and materials

Data supporting the findings of this study are available from the corresponding author upon reasonable request.

Ruano, M., Bedford, M., Kelemen, D., & Ferro, V. A. (2026). Establishing a chicken embryo model for studying infection control of a novel lipid nanoparticle. *International Journal of Pharmaceutics*, 690, Article 126569. <https://doi.org/10.1016/j.ijpharm.2026.126569>. For the purpose of open access, a CC BY 4.0 licence has been applied.

Funding

This work was supported by AB Vista, ABITEC Corporation, and the University of Strathclyde.

Copyright

© Marta Ruano 2025.

Ruano, M., Bedford, M., Kelemen, D., & Ferro, V. A. (2026). Establishing a chicken embryo model for studying infection control of a novel lipid nanoparticle. *International Journal of Pharmaceutics*, 690, Article 126569. <https://doi.org/10.1016/j.ijpharm.2026.126569>. For the purpose of open access, a CC BY 4.0 licence has been applied.

- Abo-zeid, Y., Amer, A., El-Houssieny, B., Mahmoud, M., Sakran, W., 2021. Overview on bacterial resistance and nanoparticles to overcome bacterial resistance. *J. Adv. Pharm. Res.* 0, 0–0. <https://doi.org/10.21608/aprh.2021.76488.1131>
- Aljihani, S.A., Alehaideb, Z., Alarfaj, R.E., Alghoribi, M.F., Akiel, M.A., Alenazi, T.H., Al-Fahad, A.J., Al Tamimi, S.M., Albakr, T.M., Alshehri, A., Alyahya, S.M., Yassin, A.E.B., Halwani, M.A., 2020. Enhancing azithromycin antibacterial activity by encapsulation in liposomes/liposomal-N-acetylcysteine formulations against resistant clinical strains of *Escherichia coli*. *Saudi J. Biol. Sci.* 27, 3065–3071. <https://doi.org/10.1016/j.sjbs.2020.09.012>
- Barnoy, S., Gancz, H., Zhu, Y., Honnold, C.L., Zurawski, D.V., Venkatesan, M.M., 2017. The *Galleria mellonella* larvae as an *in vivo* model for evaluation of *Shigella* virulence. *Gut Microbes* 8, 335–350. <https://doi.org/10.1080/19490976.2017.1293225>
- Beloqui, A., Solinís, M.Á., Rodríguez-Gascón, A., Almeida, A.J., Prétat, V., 2016. Nanostructured lipid carriers: Promising drug delivery systems for future clinics. *Nanomedicine Nanotechnol. Biol. Med.* 12, 143–161. <https://doi.org/10.1016/j.nano.2015.09.004>
- Buhr, C.R., Wiesmann, N., Tanner, R.C., Brieger, J., Eckrich, J., 2020. The Chorioallantoic Membrane Assay in Nanotoxicological Research—An Alternative for *In Vivo* Experimentation. *Nanomaterials* 10, 2328. <https://doi.org/10.3390/nano10122328>
- Butler, K.S., Brinker, C.J., Leong, H.S., 2022. Bridging the *In Vitro* to *In Vivo* gap: Using the Chick Embryo Model to Accelerate Nanoparticle Validation and Qualification for *In Vivo* studies. *ACS Nano* 16, 19626–19650. <https://doi.org/10.1021/acsnano.2c03990>
- Byrne, J.M., Waack, U., Weinstein, E.A., Joshi, A., Shurland, S.M., Iarikov, D., Bulitta, J.B., Diep, B.A., Guina, T., Hope, W.W., Lawrenz, M.B., Lepak, A.J., Luna, B.M., Miesel, L., Phipps, A.J., Walsh, T.J., Weiss, W., Amini, T., Farley, J.J., 2020. FDA Public Workshop Summary: Advancing Animal Models for Antibacterial Drug Development. *Antimicrob. Agents Chemother.* 65, e01983-20. <https://doi.org/10.1128/AAC.01983-20>
- Castañeda, C.D., McDaniel, C.D., Abdelhamed, H., Karsi, A., Kiess, A.S., 2019. Evaluating bacterial colonization of a developing broiler embryo after *in ovo* injection with a bioluminescent bacteria. *Poult. Sci.* 98, 2997–3006. <https://doi.org/10.3382/ps/pez053>
- Chen, L., Wang, S., Feng, Y., Zhang, Jinyong, Du, Y., Zhang, Jiang, Ongeval, C.V., Ni, Y., Li, Y., 2021. Utilisation of Chick Embryo Chorioallantoic Membrane as a Model Platform for Imaging-Navigated Biomedical Research. *Cells* 10, 463. <https://doi.org/10.3390/cells10020463>
- Chintoan-Uta, C., Cassady-Cain, R.L., Al-Haideri, H., Watson, E., Kelly, D.J., Smith, D.G.E., Sparks, N.H.C., Kaiser, P., Stevens, M.P., 2015. Superoxide dismutase SodB is a protective antigen against *Campylobacter jejuni* colonisation in chickens. *Vaccine* 33, 6206–6211. <https://doi.org/10.1016/j.vaccine.2015.09.100>
- Chintoan-Uta, C., Cassady-Cain, R.L., Stevens, M.P., 2016. Evaluation of flagellum-related proteins FliD and FspA as subunit vaccines against *Campylobacter jejuni* colonisation in chickens. *Vaccine* 34, 1739–1743. <https://doi.org/10.1016/j.vaccine.2016.02.052>

Ruano, M., Bedford, M., Kelemen, D., & Ferro, V. A. (2026). Establishing a chicken embryo model for studying infection control of a novel lipid nanoparticle. *International Journal of Pharmaceutics*, 690, Article 126569. <https://doi.org/10.1016/j.ijpharm.2026.126569>. For the purpose of open access, a CC BY 4.0 licence has been applied.

- Cyphert, E., Wallat, J., Pokorski, J., Von Recum, H., 2017. Erythromycin Modification That Improves Its Acidic Stability while Optimizing It for Local Drug Delivery. *Antibiotics* 6, 11. <https://doi.org/10.3390/antibiotics6020011>
- Das, P., Ghosh, S., Nayak, B., 2021. Phyto-fabricated Nanoparticles and Their Anti-biofilm Activity: Progress and Current Status. *Front. Nanotechnol.* 3, 739286. <https://doi.org/10.3389/fnano.2021.739286>
- De Araujo Lowndes Viera, L.M., Silva, R.S., Da Silva, C.C., Presgrave, O.A.F., Boas, M.H.S.V., 2022. Comparison of the different protocols of the Hen's Egg Test-Chorioallantoic Membrane (HET-CAM) by evaluating the eye irritation potential of surfactants. *Toxicol. In Vitro* 78, 105255. <https://doi.org/10.1016/j.tiv.2021.105255>
- De Souza, J.B., Sommerfeld, S., Almeida-Souza, H.O., Vaz, E.R., Bastos, L.M., Santos, F.D.A.A., Rodrigues, A.C., Medeiros-Ronchi, A.A., Goulart, L.R., Fonseca, B.B., 2024. A new standardization for the use of chicken embryo: selection of target from the phage display library and infection. *Appl. Microbiol. Biotechnol.* 108, 412. <https://doi.org/10.1007/s00253-024-13227-x>
- Dhayer, M., Jordao, A., Dekiok, S., Cleret, D., Germain, N., Marchetti, P., 2024. Implementing Chicken Chorioallantoic Membrane (CAM) Assays for Validating Biomaterials in Tissue Engineering: Rationale and Methods. *J. Biomed. Mater. Res. B Appl. Biomater.* 112, e35496. <https://doi.org/10.1002/jbm.b.35496>
- Dinos, G.P., 2017. The macrolide antibiotic renaissance. *Br. J. Pharmacol.* 174, 2967–2983. <https://doi.org/10.1111/bph.13936>
- Dolka, B., Czopowicz, M., Dolka, I., Szeleszczuk, P., 2022. Chicken embryo lethality assay for determining the lethal dose, tissue distribution and pathogenicity of clinical *Enterococcus cecorum* isolates from poultry. *Sci. Rep.* 12, 10675. <https://doi.org/10.1038/s41598-022-14900-9>
- García-Gareta, E., Binkowska, J., Kohli, N., Sharma, V., 2020. Towards the Development of a Novel Ex Ovo Model of Infection to Pre-Screen Biomaterials Intended for Treating Chronic Wounds. *J. Funct. Biomater.* 11, 37. <https://doi.org/10.3390/jfb11020037>
- Gomes, M.C., Mostowy, S., 2020. The Case for Modeling Human Infection in Zebrafish. *Trends Microbiol.* 28, 10–18. <https://doi.org/10.1016/j.tim.2019.08.005>
- González-Fernández, F.M., Bianchera, A., Gasco, P., Nicoli, S., Pescina, S., 2021. Lipid-Based Nanocarriers for Ophthalmic Administration: Towards Experimental Design Implementation. *Pharmaceutics* 13, 447. <https://doi.org/10.3390/pharmaceutics13040447>
- Hemmati, J., Chegini, Z., Arabestani, M.R., 2023. Niosomal-Based Drug Delivery Platforms: A Promising Therapeutic Approach to Fight *Staphylococcus aureus* Drug Resistance. *J. Nanomater.* 2023, 1–18. <https://doi.org/10.1155/2023/5298565>
- Jacobson, K.H., Gunsolus, I.L., Kuech, T.R., Troiano, J.M., Melby, E.S., Lohse, S.E., Hu, D., Chrisler, W.B., Murphy, C.J., Orr, G., Geiger, F.M., Haynes, C.L., Pedersen, J.A., 2015. Lipopolysaccharide Density and Structure Govern the Extent and Distance of Nanoparticle Interaction with Actual and Model Bacterial Outer Membranes. *Environ. Sci. Technol.* 49, 10642–10650. <https://doi.org/10.1021/acs.est.5b01841>

Ruano, M., Bedford, M., Kelemen, D., & Ferro, V. A. (2026). Establishing a chicken embryo model for studying infection control of a novel lipid nanoparticle. *International Journal of Pharmaceutics*, 690, Article 126569. <https://doi.org/10.1016/j.ijpharm.2026.126569>. For the purpose of open access, a CC BY 4.0 licence has been applied.

- Jakubek, Z.J., Chen, S., Zaifman, J., Tam, Y.Y.C., Zou, S., 2023. Lipid Nanoparticle and Liposome Reference Materials: Assessment of Size Homogeneity and Long-Term -70 °C and 4 °C Storage Stability. *Langmuir* 39, 2509–2519. <https://doi.org/10.1021/acs.langmuir.2c02657>
- Jung, D., Jang, S., Park, D., Bae, N.H., Han, C.S., Ryu, S., Lim, E.-K., Lee, K.G., 2025. Automated Microfluidic Systems Facilitating the Scalable and Reliable Production of Lipid Nanoparticles for Gene Delivery. *BioChip J.* 19, 79–90. <https://doi.org/10.1007/s13206-024-00182-y>
- Kalmar, I., Berndt, A., Yin, L., Chiers, K., Sachse, K., Vanrompay, D., 2015. Host–pathogen interactions in specific pathogen-free chickens following aerogenous infection with *Chlamydia psittaci* and *Chlamydia abortus*. *Vet. Immunol. Immunopathol.* 164, 30–39. <https://doi.org/10.1016/j.vetimm.2014.12.014>
- Klymchenko, A.S., Liu, F., Collot, M., Anton, N., 2021. Dye-Loaded Nanoemulsions: Biomimetic Fluorescent Nanocarriers for Bioimaging and Nanomedicine. *Adv. Healthc. Mater.* 10, 2001289. <https://doi.org/10.1002/adhm.202001289>
- Kovacevic, A., Savic, S., Vuleta, G., Müller, R.H., Keck, C.M., 2011. Polyhydroxy surfactants for the formulation of lipid nanoparticles (SLN and NLC): Effects on size, physical stability and particle matrix structure. *Int. J. Pharm.* 406, 163–172. <https://doi.org/10.1016/j.ijpharm.2010.12.036>
- Krawczyk, S.J., Leśniczak-Staszak, M., Gowin, E., Szaflarski, W., 2024. Mechanistic Insights into Clinically Relevant Ribosome-Targeting Antibiotics. *Biomolecules* 14, 1263. <https://doi.org/10.3390/biom14101263>
- Kue, C.S., Tan, K.Y., Lam, M.L., Lee, H.B., 2015. Chick embryo chorioallantoic membrane (CAM): an alternative predictive model in acute toxicological studies for anti-cancer drugs. *Exp. Anim.* 64, 129–138. <https://doi.org/10.1538/expanim.14-0059>
- Kundeková, B., Máčajová, M., Meta, M., Čavarga, I., Bilčík, B., 2021. Chorioallantoic Membrane Models of Various Avian Species: Differences and Applications. *Biology* 10, 301. <https://doi.org/10.3390/biology10040301>
- Lacic, B., Beh, C., Sarkar, S., Yap, S.-L., Cardoso, P., Valery, C., Hung, A., Jones, N.C., Hoffmann, S.V., Blanch, E.W., Dyett, B., Conn, C.E., 2025. Cubosome lipid nanocarriers for delivery of ultra-short antimicrobial peptides. *J. Colloid Interface Sci.* 677, 1080–1097. <https://doi.org/10.1016/j.jcis.2024.07.232>
- Lopes, L.Q.S., De Almeida Vaucher, R., Giongo, J.L., Gündel, A., Santos, R.C.V., 2019a. Characterisation and anti-biofilm activity of glycerol monolaurate nanocapsules against *Pseudomonas aeruginosa*. *Microb. Pathog.* 130, 178–185. <https://doi.org/10.1016/j.micpath.2019.03.007>
- Lopes, L.Q.S., De Oliveira, P.S.B., De Souza Filho, W.P., De Almeida Vaucher, R., Giongo, J.L., Sagrillo, M.R., Santos, R.C.V., 2019b. Glycerol monolaurate nanocapsules for biomedical applications: in vitro toxicological studies. *Naunyn. Schmiedebergs Arch. Pharmacol.* 392, 1131–1140. <https://doi.org/10.1007/s00210-019-01663-w>
- Lopes, L.Q.S., Santos, C.G., De Almeida Vaucher, R., Gende, L., Raffin, R.P., Santos, R.C.V., 2016. Evaluation of antimicrobial activity of glycerol monolaurate nanocapsules against American foulbrood disease agent and toxicity on bees. *Microb. Pathog.* 97, 183–188. <https://doi.org/10.1016/j.micpath.2016.05.014>
- Lotz, C., 2016. Alternative methods for the replacement of eye irritation testing. *ALTEX* 55–67. <https://doi.org/10.14573/altex.1508241>

Ruano, M., Bedford, M., Kelemen, D., & Ferro, V. A. (2026). Establishing a chicken embryo model for studying infection control of a novel lipid nanoparticle. *International Journal of Pharmaceutics*, 690, Article 126569. <https://doi.org/10.1016/j.ijpharm.2026.126569>. For the purpose of open access, a CC BY 4.0 licence has been applied.

- Markova, N., Cairns, S., Jankevics-Jones, H., Kaszuba, M., Caputo, F., Parot, J., 2021. Biophysical Characterization of Viral and Lipid-Based Vectors for Vaccines and Therapeutics with Light Scattering and Calorimetric Techniques. *Vaccines* 10, 49. <https://doi.org/10.3390/vaccines10010049>
- Mehnert, W., 2001. Solid lipid nanoparticles Production, characterization and applications. *Adv. Drug Deliv. Rev.* 47, 165–196. [https://doi.org/10.1016/S0169-409X\(01\)00105-3](https://doi.org/10.1016/S0169-409X(01)00105-3)
- Meikle, T.G., Dharmadana, D., Hoffmann, S.V., Jones, N.C., Drummond, C.J., Conn, C.E., 2021. Analysis of the structure, loading and activity of six antimicrobial peptides encapsulated in cubic phase lipid nanoparticles. *J. Colloid Interface Sci.* 587, 90–100. <https://doi.org/10.1016/j.jcis.2020.11.124>
- Modi, S.K., Gaur, S., Sengupta, M., Singh, M.S., 2023. Mechanistic insights into nanoparticle surface-bacterial membrane interactions in overcoming antibiotic resistance. *Front. Microbiol.* 14, 1135579. <https://doi.org/10.3389/fmicb.2023.1135579>
- Motsoene, F., Abrahamse, H., Dhilip Kumar, S.S., 2023. Multifunctional lipid-based nanoparticles for wound healing and antibacterial applications: A review. *Adv. Colloid Interface Sci.* 321, 103002. <https://doi.org/10.1016/j.cis.2023.103002>
- Naik, M., Brahma, P., Dixit, M., 2018. A Cost-Effective and Efficient Chick Ex-Ovo CAM Assay Protocol to Assess Angiogenesis. *Methods Protoc.* 1, 19. <https://doi.org/10.3390/mps1020019>
- Nanoparticles characterization using the CAM assay, 2019. , in: *The Enzymes*. Elsevier, pp. 129–160. <https://doi.org/10.1016/bs.enz.2019.09.001>
- Nath, A.G., Dubey, P., Kumar, A., Vaiphei, K.K., Rosenholm, J.M., Bansal, K.K., Gulbake, A., 2024. Recent Advances in the Use of Cubosomes as Drug Carriers with Special Emphasis on Topical Applications. *J. Lipids* 2024, 2683466. <https://doi.org/10.1155/2024/2683466>
- National Institute of Environmental Health Sciences., 2006. *In Vitro Ocular Toxicity Methods for Identifying Severe Irritants and Corrosives. (ICCVAM Test Method Evaluation Report No. 07-4517.)*. Research Triangle Park, NC.
- Niamprem, P., Srinivas, S.P., Tiyaboonchai, W., 2019. Penetration of Nile red-loaded nanostructured lipid carriers (NLCs) across the porcine cornea. *Colloids Surf. B Biointerfaces* 176, 371–378. <https://doi.org/10.1016/j.colsurfb.2019.01.018>
- Patiño-Morales, C.C., Jaime-Cruz, R., Ramírez-Fuentes, T.C., Villavicencio-Guzmán, L., Salazar-García, M., 2023. Technical Implications of the Chicken Embryo Chorioallantoic Membrane Assay to Elucidate Neuroblastoma Biology. *Int. J. Mol. Sci.* 24, 14744. <https://doi.org/10.3390/ijms241914744>
- Patra, M.K., Sanchu, V., Ngullie, E., Hajra, D.K., Deka, B.C., 2016. Influence of egg weight on fertility and hatchability of backyard poultry varieties maintained under institutional farm conditions. *Indian J. Anim. Sci.* 86. <https://doi.org/10.56093/ijans.v86i8.60760>
- Peebles, E.D., Brake, J., 1987. Eggshell Quality and Hatchability in Broiler Breeder Eggs ,. *Poult. Sci.* 66, 596–604. <https://doi.org/10.3382/ps.0660596>
- Perrigue, P.M., Murray, R.A., Mielcarek, A., Henschke, A., Moya, S.E., 2021. Degradation of Drug Delivery Nanocarriers and Payload Release: A Review of Physical Methods for Tracing Nanocarrier Biological Fate. *Pharmaceutics* 13, 770. <https://doi.org/10.3390/pharmaceutics13060770>

Ruano, M., Bedford, M., Kelemen, D., & Ferro, V. A. (2026). Establishing a chicken embryo model for studying infection control of a novel lipid nanoparticle. *International Journal of Pharmaceutics*, 690, Article 126569. <https://doi.org/10.1016/j.ijpharm.2026.126569>. For the purpose of open access, a CC BY 4.0 licence has been applied.

- Platon, V.-M., Dragoi, B., Marin, L., 2022. Erythromycin Formulations—A Journey to Advanced Drug Delivery. *Pharmaceutics* 14, 2180. <https://doi.org/10.3390/pharmaceutics14102180>
- Ramakrishnan, M.A., 2016. Determination of 50% endpoint titer using a simple formula. *World J. Virol.* 5, 85. <https://doi.org/10.5501/wjv.v5.i2.85>
- Ranghar, S., Sirohi, P., Verma, P., Agarwal, V., 2013. Nanoparticle-based drug delivery systems: promising approaches against infections. *Braz. Arch. Biol. Technol.* 57, 209–222. <https://doi.org/10.1590/S1516-89132013005000011>
- Reed, L.J., Muench, H., 1938. A SIMPLE METHOD OF ESTIMATING FIFTY PER CENT ENDPOINTS. *Am. J. Epidemiol.* 27, 493–497. <https://doi.org/10.1093/oxfordjournals.aje.a118408>
- Rivero, M.N., Lenze, M., Izaguirre, M., Pérez Damonte, S.H., Aguilar, A., Wikinski, S., Gutiérrez, M.L., 2021. Comparison between HET-CAM protocols and a product use clinical study for eye irritation evaluation of personal care products including cosmetics according to their surfactant composition. *Food Chem. Toxicol.* 153, 112229. <https://doi.org/10.1016/j.fct.2021.112229>
- Ruano, M., Sut, T.N., Tan, S.W., Mullen, A.B., Kelemen, D., Ferro, V.A., Jackman, J.A., 2025. Solvent-Free Microfluidic Fabrication of Antimicrobial Lipid Nanoparticles. *ACS Appl. Bio Mater.* 8, 2194–2203. <https://doi.org/10.1021/acsabm.4c01747>
- Schulze, J., Schöne, L., Ayoub, A.M., Librizzi, D., Amin, M.U., Engelhardt, K., Yousefi, B.H., Bender, L., Schaefer, J., Preis, E., Schulz-Siegmund, M., Wölk, C., Bakowsky, U., 2023. Modern Photodynamic Glioblastoma Therapy Using Curcumin- or Parietin-Loaded Lipid Nanoparticles in a CAM Model Study. *ACS Appl. Bio Mater.* 6, 5502–5514. <https://doi.org/10.1021/acsabm.3c00695>
- Singh, J., Nayak, P., 2023. pH -responsive polymers for drug delivery: Trends and opportunities. *J. Polym. Sci.* 61, 2828–2850. <https://doi.org/10.1002/pol.20230403>
- Smail, S.S., 2024. Ex Vivo Irritation Evaluation of a Novel Brimonidine Nanoemulsion Using the Hen's Egg Test on Chorioallantoic Membrane (HET-CAM). *Cureus.* <https://doi.org/10.7759/cureus.68280>
- Vairo, C., Basas, J., Pastor, M., Palau, M., Gomis, X., Almirante, B., Gainza, E., Hernandez, R.M., Igartua, M., Gavaldà, J., Gainza, G., 2020. In vitro and in vivo antimicrobial activity of sodium colistimethate and amikacin-loaded nanostructured lipid carriers (NLC). *Nanomedicine Nanotechnol. Biol. Med.* 29, 102259. <https://doi.org/10.1016/j.nano.2020.102259>
- Valdivia, R.H., Hromockyj, A.E., Monack, D., Ramakrishnan, L., Falkow, S., 1996. Applications for green fluorescent protein (GFP) in the study of hostpathogen interactions. *Gene* 173, 47–52. [https://doi.org/10.1016/0378-1119\(95\)00706-7](https://doi.org/10.1016/0378-1119(95)00706-7)
- Vandoolaeghe, P., Rennie, A.R., Campbell, R.A., Nylander, T., 2009. Neutron Reflectivity Studies of the Interaction of Cubic-Phase Nanoparticles with Phospholipid Bilayers of Different Coverage. *Langmuir* 25, 4009–4020. <https://doi.org/10.1021/la802766n>
- Vauthier, C., Bouchemal, K., 2009. Methods for the Preparation and Manufacture of Polymeric Nanoparticles. *Pharm. Res.* 26, 1025–1058. <https://doi.org/10.1007/s11095-008-9800-3>
- Vázquez-Laslop, N., Mankin, A.S., 2018. How Macrolide Antibiotics Work. *Trends Biochem. Sci.* 43, 668–684. <https://doi.org/10.1016/j.tibs.2018.06.011>

Ruano, M., Bedford, M., Kelemen, D., & Ferro, V. A. (2026). Establishing a chicken embryo model for studying infection control of a novel lipid nanoparticle. *International Journal of Pharmaceutics*, 690, Article 126569. <https://doi.org/10.1016/j.ijpharm.2026.126569>. For the purpose of open access, a CC BY 4.0 licence has been applied.

- Victorelli, F.D., Cardoso, V.M.D.O., Ferreira, N.N., Calixto, G.M.F., Fontana, C.R., Baltazar, F., Gremião, M.P.D., Chorilli, M., 2020. Chick embryo chorioallantoic membrane as a suitable in vivo model to evaluate drug delivery systems for cancer treatment: A review. *Eur. J. Pharm. Biopharm.* 153, 273–284. <https://doi.org/10.1016/j.ejpb.2020.06.010>
- Villani, S., Calcagnile, M., Demitri, C., Alifano, P., 2025. Galleria mellonella (Greater Wax Moth) as a Reliable Animal Model to Study the Efficacy of Nanomaterials in Fighting Pathogens. *Nanomaterials* 15, 67. <https://doi.org/10.3390/nano15010067>
- Voicu, G., Grumezescu, V., Andronescu, E., Grumezescu, A.M., Ficai, A., Ficai, D., Ghitulica, C.D., Gheorghe, I., Chifiriuc, M.C., 2013. Caprolactam-silica network, a strong potentiator of the antimicrobial activity of kanamycin against Gram-positive and Gram-negative bacterial strains. *Int. J. Pharm.* 446, 63–69. <https://doi.org/10.1016/j.ijpharm.2013.02.011>
- Wang, Y., Xue, W., Pustovalova, M., Kuzmin, D.V., Leonov, S., 2025. Chick Embryo Chorioallantoic Membrane (CAM) Model for Cancer Studies and Drug Evaluation. *Front. Biosci.-Landmark* 30, 37456. <https://doi.org/10.31083/FBL37456>
- Warncke, P., Fink, S., Wiegand, C., Hipler, U.-C., Fischer, D., 2020. A shell-less hen's egg test as infection model to determine the biocompatibility and antimicrobial efficacy of drugs and drug formulations against *Pseudomonas aeruginosa*. *Int. J. Pharm.* 585, 119557. <https://doi.org/10.1016/j.ijpharm.2020.119557>
- Zaidi, S.A., 2016. Molecular imprinted polymers as drug delivery vehicles. *Drug Deliv.* 23, 2262–2271. <https://doi.org/10.3109/10717544.2014.970297>
- Zou, W., McAdorey, A., Yan, H., Chen, W., 2023. Nanomedicine to Overcome Antimicrobial Resistance: Challenges and Prospects. *Nanomed.* 18, 471–484. <https://doi.org/10.2217/nnm-2023-0022>

Establishing a chicken embryo model for studying infection control of a novel lipid nanoparticle

Marta Ruano^{1*}, Mike Bedford², Donald Kelemen³, Valerie A. Ferro¹

¹Strathclyde Institute of Pharmacy & Biomedical Sciences, University of Strathclyde,
161
Cathedral Street, Glasgow, G4 0RE, United Kingdom

²AB Vista, Woodstock Court, Marlborough, Wiltshire SN8 4AN, UK

³ABITEC Corporation, 501 W 1st Ave, Columbus, OH 43215, United States

*Address correspondence to:

E-mail: marta.ruano-aldea@strath.ac.uk (M.R.)

Supporting Information for: *Establishing a chicken embryo model for studying infection control of a novel lipid nanoparticle*

S1. Additional information for Preparation of GDB4 nanoparticles labelled with fluorescent dyes and encapsulation of erythromycin (ERY)

S2.1. Encapsulation of erythromycin (ERY)

ERY was dissolved in the preheated lipid solvent mixture at its maximum solubility ($\sim 0.6 \text{ mg mL}^{-1}$). The lipid and aqueous phases were combined in the microfluidic device under the conditions described in the method published for the fabrication of empty GDB4. Unencapsulated ERY was removed by centrifugation using Amicon Ultra filters (100 kDa MWCO, 8,000 rpm, 30 min). The supernatant containing ERY-loaded nanoparticles (GDB4-ERY) was stored at room temperature, while the pellet was resuspended in PBS containing 1 mM bile salts for subsequent ERY quantification by LC-MS.

S2.2. Preparation of GDB4 nanoparticles labelled with fluorescent dyes

NR (0.02 mg/10 mL lipid) was dissolved in the lipid solvent mixture and processed with the aqueous phase through the microfluidic device at 40 °C (9:1 aqueous-to-lipid ratio, 10 mL min⁻¹) to generate GDB4-NR nanoparticles. FITC (1 mg in 10 mL aqueous) was dissolved in the aqueous phase and combined with the lipid phase under the same microfluidic conditions to produce GDB4-FITC nanoparticles. Unencapsulated FITC was removed by dialysis (12–14 kDa MWCO) against 500 mL PBS at 37 °C and 200 rpm for 24 h.

All formulations were stored at room temperature and characterized for physicochemical properties, encapsulation efficiency, and fluorescence stability as reported in the Supplementary Tables S1–S3 and Figures S1–S3.

S2. Additional information for characterization

S2.1 LNP characterization

Hydrodynamic diameter (Dh), polydispersity index (PDI), and ζ -potential (ZP) of lipid nanoparticle (LNP) formulations were determined by dynamic light scattering (DLS) and electrophoretic light scattering using a Zetasizer Nano ZS (Malvern Instruments, Malvern, UK). Samples were diluted 1:10 in deionised water to a final lipid concentration of 1 mg mL⁻¹ prior to analysis. Measurements were performed in triplicate at 25 °C, and results are reported as mean \pm standard deviation.

S2.2 Quantification of encapsulated erythromycin (ERY)

ERY quantification was performed by liquid chromatography–mass spectrometry (LC–MS) using an Advion UHPLC–MS system (Pure and Applied Chemistry Department, University of Strathclyde). Samples were prepared in 250 μ L vial inserts (Agilent), with 100 μ L aliquots transferred to HPLC vials for analysis.

Chromatographic separation was achieved using a Phenomenex Kinetix C18 reverse-phase column (2.6 μ m, 100 Å) operated at room temperature. The mobile phase consisted of Solvent A (0.1% v/v formic acid in Milli-Q water) and Solvent B (acetonitrile, ACN). A linear gradient was applied, starting at 95% A and 5% B, transitioning to 5% A and 95% B at 2.5 min, held until 3.6 min, and returning to initial conditions at 4 min. The flow rate was 1 mL min⁻¹ with an injection volume of 10 μ L. ERY was detected at 220 nm.

ERY concentration was determined using an external calibration curve and quantified in both the supernatant and pellet fractions to ensure complete mass balance following separation (Platon et al., 2022; S. Zgoulli, V. Grek, G. Barre, G. G., 1999) . The pellet was resuspended in the same solvent prior to analysis.

Encapsulation efficiency (EE) was calculated as:

$$EE (\%) = [(ERY_{\text{total}} - ERY_{\text{supernatant}}) / ERY_{\text{total}}] \times 100 \quad \text{Eq. S 1}$$

S2.3 Quantification of encapsulated FITC

Encapsulated fluorescein isothiocyanate (FITC) was quantified by UV–visible spectroscopy using a Jenway 6310 spectrophotometer (Barloworld Scientific Ltd., Dunmow, UK). Absorbance measurements were performed in Milli-Q water at the

FITC absorption maximum. FITC concentrations were calculated by interpolation from a calibration curve constructed using standards ranging from 0 to 1 mg L⁻¹.

Encapsulation efficiency was calculated based on the amount of FITC retained within the LNPs following dialysis, where FITC_{dialysate} corresponds to unencapsulated dye removed during purification. All measurements were performed in triplicate and are reported as mean ± standard deviation (Natarajan et al., 2017; Thorball, 1981).

Encapsulation efficiency (EE) was calculated as:

$$EE (\%) = [(FITC_{total} - FITC_{dialysate}) / FITC_{total}] \times 100 \quad \text{Eq. S 2}$$

S3. In vitro antimicrobial assays

Staphylococcus aureus and *Salmonella enterica* subsp. *enterica* serovar Enteritidis were cultured overnight in Mueller–Hinton broth (MHB) at 37 °C under aerobic conditions. Overnight cultures were diluted in fresh MHB and grown to the exponential phase (OD₆₀₀ ≈ 0.3), as measured using a UV–vis spectrophotometer. Bacterial cells were collected by centrifugation (1500 × g, 10 min), washed three times with phosphate-buffered saline (PBS), and resuspended in MHB. Cell suspensions were adjusted to OD₆₀₀ = 0.1, corresponding to approximately 1 × 10⁷ CFU mL⁻¹ for *S. aureus* (Zoraghi et al., 2011), and used within 15 min.

Minimum inhibitory concentration (MIC) assays were performed using the broth microdilution method in accordance with NCCLS and BSAC guidelines (Elshikh et al., 2016; Kowalska-Krochmal and Dudek-Wicher, 2021). Briefly, two-fold serial dilutions of LNP formulations were prepared in PBS in 96-well microplates, covering a concentration range of 40 µg mL⁻¹ to 10 mg mL⁻¹ (100 µL per well). Each well was inoculated with 5 µL of bacterial suspension (1 × 10⁵ CFU mL⁻¹), resulting in a final bacterial density of 5 × 10⁴ CFU per well.

Plates were incubated at 37 °C for 24 h, after which bacterial growth was quantified by measuring OD₆₀₀ using a microplate reader. Bacterial viability was expressed relative to untreated controls. MIC₅₀ values were determined by fitting concentration–response data to a four-parameter logistic (4PL) model and defined as the

nanoparticle concentration required to inhibit bacterial growth by 50% (Andrews, 2001).

Table S1. Control groups tested in the chicken embryo model optimized

Control groups	Description
Non-treatment control	Embryos received sterile PBS only, serving as a baseline for natural survival.
PBS control	Assessed potential toxicity of the buffer used in treatments or bacterial suspensions.
Bile salts control	Evaluated biocompatibility of bile salts and their impact on embryo viability.
PBS + broth control	Verified that the bacterial growth medium (MHB) did not affect survival.
Formulation/antibiotic alone, with no infection	Assessed toxicity and biocompatibility of formulations or free antibiotics in the absence of bacteria.

Table S2. Treatment groups tested in the chicken embryo model- optimized

Treatment	Description	C (mg mL⁻¹)
Antibiotic treatment	Embryos inoculated with bacteria at LD50 and treated with free ERY (1 mg mL ⁻¹) to assess standalone antibiotic efficacy.	1
Formulation treatment	Embryos inoculated with bacteria and treated with antibiotic-free formulations (e.g., bile-salt) to evaluate intrinsic bacteriostatic effects and biocompatibility.	6.7
Formulations with encapsulated antibiotic	Embryos inoculated with bacteria and treated with bile-salt-based formulations encapsulating ERY (6.7 mg mL ⁻¹) to assess enhanced efficacy, sustained release, and reduced toxicity compared to free antibiotic.	6.7

Table S3. Physicochemical characteristics of freshly prepared GDB4 lipid nanoparticle formulations.

Hydrodynamic diameter (D_h), polydispersity index (PDI), and ζ -potential (ZP) of blank GDB4, ERY-loaded (GDB4-ERY), FITC-labelled (GDB4-FITC), and Nile Red-labelled (GDB4-NR) nanoparticles. Data are presented as mean \pm SD ($n = 3$).

Sample	$D_h \pm SD$ / nm	PDI \pm SD	ζ-potential \pm SD / mV
GDB4	252.5 \pm 14.6	0.28 \pm 0.01	-29.0 \pm 3.0
GDB4-ERY	259.2 \pm 5.2	0.26 \pm 0.02	-38.8 \pm 4.1
GDB4-FITC	243.4 \pm 4.0	0.38 \pm 0.08	-55.5 \pm 1.4
GDB4-NR	231.5 \pm 11.4	0.23 \pm 0.09	-33.5 \pm 3.0

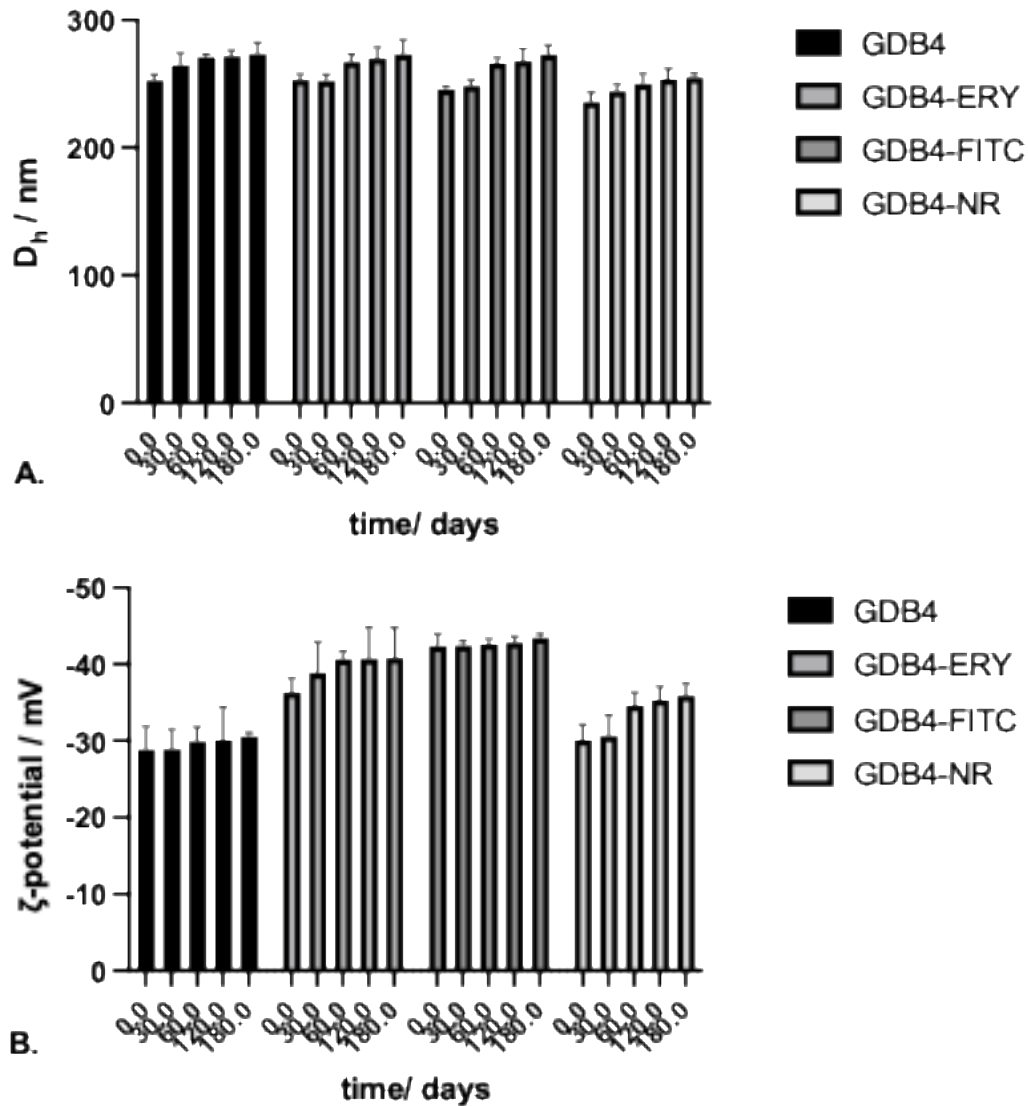


Fig. S1. Characterization of lipid nanoparticle formulations. (A) Hydrodynamic diameter (D_h , nm) and (B) ζ -potential (mV) of GDB4, GDB4-ERY, GDB4-FITC, and GDB4-NR measured after 0, 30, 60, 120 and 180 days of storage. Values are expressed as mean \pm SD ($n = 20$); Negative ζ -potentials are plotted upwards. Statistical analysis was performed using the Kruskal–Wallis test. Kruskal–Wallis test indicated significant differences ($H = 17.47$, $p = 0.0006$).

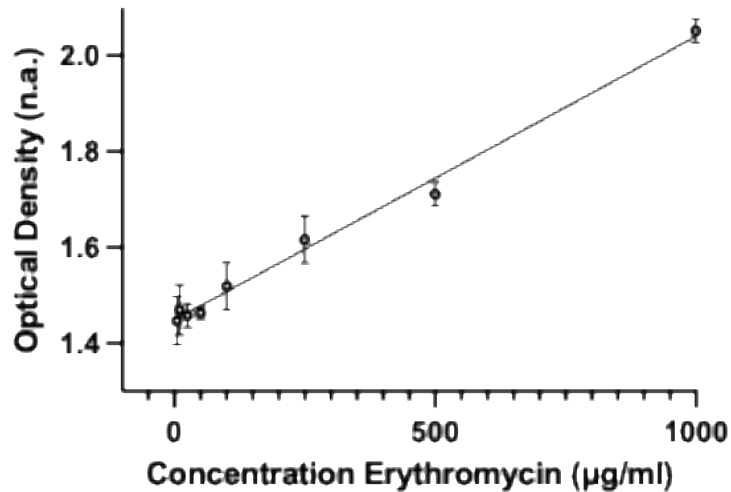


Fig. S2. Calibration curve for erythromycin (ERY) quantification by LC-MS. Signal intensity plotted as a function of ERY concentration ($\mu\text{g mL}^{-1}$). Data represent mean \pm SD of three independent measurements ($n = 3$). Linear regression analysis demonstrated a strong correlation between signal intensity and ERY concentration ($R^2 = 0.9882$, $p < 0.0001$).

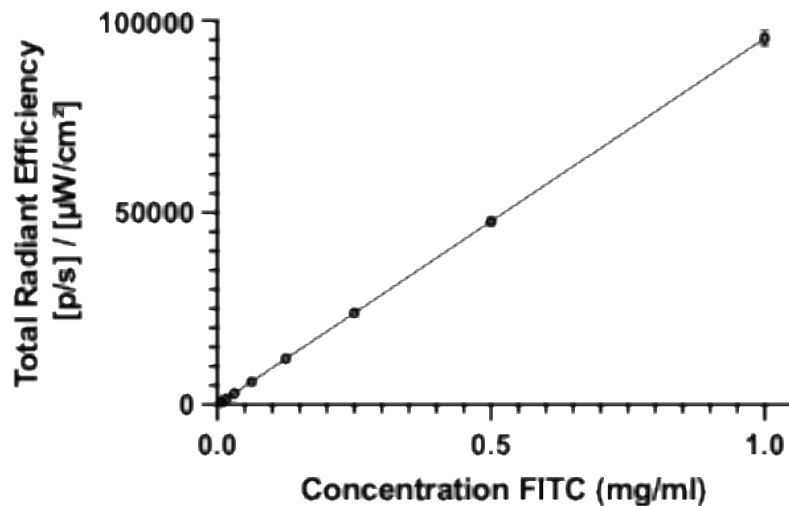


Fig. S3. Calibration curve for FITC quantification by fluorescence spectroscopy. Fluorescence intensity plotted as a function of FITC concentration ($\mu\text{g mL}^{-1}$). Data are presented as mean \pm SD ($n = 3$). Linear regression showed excellent linearity over the tested concentration range ($R^2 = 0.9999$, $p < 0.0001$).

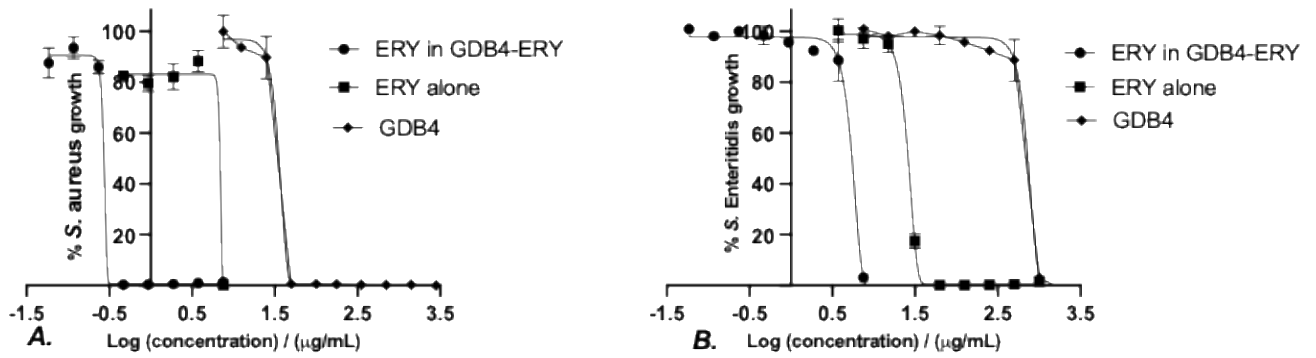


Fig. S4. *In vitro* antibacterial activity of GDB4 lipid nanoparticle formulations. Growth inhibition curves for (A) *Staphylococcus aureus* and (B) *Salmonella Enteritidis* following 24 h exposure to empty GDB4 nanoparticles, free erythromycin (ERY), or ERY-loaded GDB4 nanoparticles (GDB4-ERY). Data are expressed as mean \pm SD (n = 3). MIC₅₀ values were determined by four-parameter logistic regression.

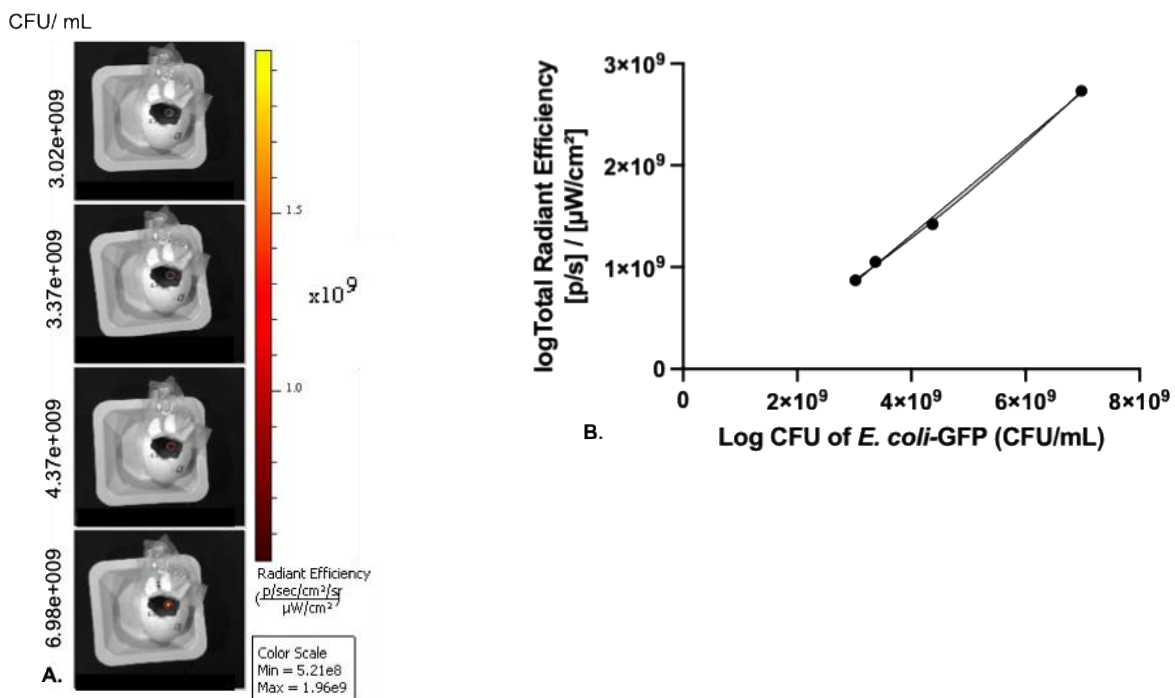


Fig. S5. *In vivo* IVIS fluorescence imaging of GFP-expressing *E. coli* JM105. (A) Representative images showing increasing GFP fluorescence with increasing bacterial inoculum. (B) Correlation between fluorescence intensity (Radiant Efficiency [p/s]/[µW cm⁻²]) and bacterial load (log CFU m L⁻¹). Data are presented as mean \pm SD (n = 10). Linear regression demonstrates a strong linear relationship between

fluorescence signal and bacterial concentration ($R^2 = 0.9971$, $p < 0.0001$), validating IVIS imaging for non-invasive quantification of *E. coli in ovo*.

Bibliography

- Andrews, J.M., 2001. Determination of minimum inhibitory concentrations. *J. Antimicrob. Chemother.* 48, 5–16. https://doi.org/10.1093/jac/48.suppl_1.5
- Elshikh, M., Ahmed, S., Funston, S., Dunlop, P., McGaw, M., Marchant, R., Banat, I.M., 2016. Resazurin-based 96-well plate microdilution method for the determination of minimum inhibitory concentration of biosurfactants. *Biotechnol. Lett.* 38, 1015–1019. <https://doi.org/10.1007/s10529-016-2079-2>
- Kowalska-Krochmal, B., Dudek-Wicher, R., 2021. The Minimum Inhibitory Concentration of Antibiotics: Methods, Interpretation, Clinical Relevance. *Pathogens* 10, 165. <https://doi.org/10.3390/pathogens10020165>
- Natarajan, R., Northrop, N., Yamamoto, B., 2017. Fluorescein Isothiocyanate (FITC)-Dextran Extravasation as a Measure of Blood-Brain Barrier Permeability. *Curr. Protoc. Neurosci.* 79. <https://doi.org/10.1002/cpns.25>
- Platon, V.-M., Dragoi, B., Marin, L., 2022. Erythromycin Formulations—A Journey to Advanced Drug Delivery. *Pharmaceutics* 14, 2180. <https://doi.org/10.3390/pharmaceutics14102180>
- S. Zgoulli, V. Grek, G. Barre, G. G., 1999. Microencapsulation of erythromycin and clarithromycin using a spray-drying technique. *J. Microencapsul.* 16, 565–571. <https://doi.org/10.1080/026520499288762>
- Thorball, N., 1981. FITC-Dextran tracers in microcirculatory and permeability studies using combined fluorescence stereo microscopy, fluorescence light microscopy and electron microscopy. *Histochemistry* 71, 209–233. <https://doi.org/10.1007/BF00507826>
- Zoraghi, R., See, R.H., Axerio-Cilies, P., Kumar, N.S., Gong, H., Moreau, A., Hsing, M., Kaur, S., Swayze, R.D., Worrall, L., Amandoron, E., Lian, T., Jackson, L., Jiang, J., Thorson, L., Labriere, C., Foster, L., Brunham, R.C., McMaster, W.R., Finlay, B.B., Strynadka, N.C., Cherkasov, A., Young, R.N., Reiner, N.E., 2011. Identification of Pyruvate Kinase in Methicillin-Resistant *Staphylococcus aureus* as a Novel Antimicrobial Drug Target. *Antimicrob. Agents Chemother.* 55, 2042–2053. <https://doi.org/10.1128/AAC.01250-10>